IDENTIFICATION OF NOVEL INTRACELLULAR MECHANISMS IN DEVELOPMENTAL SPINE PRUNING THROUGH ANKYRIN B

Elliott V. Wyatt

A thesis submitted to the faculty at the University of North Carolina at Chapel Hill in partial fulfillment of the requirements for the degree of Masters of Science in the School of Medicine (Neuroscience)

Chapel Hill
2019

Approved by:

Patricia F. Maness

Richard Cheney

Stephanie Gupton

Kathryn Reissner

Damaris Lorenzo

ABSTRACT

Elliott V. Wyatt: Identification of novel intracellular mechanisms in developmental spine pruning through Ankyrin B.
(Under the direction of Patricia F. Maness)

Dendritic spines are the predominant site of glutamatergic inputs throughout the brain. Regulation of spines is therefore critical for refining cortical networks. This research sought to define mechanisms for determining spine fate during developmental synapse remodeling. The central hypothesis is that NrCAM requires intracellular interactions within the spine to promote Semaphorin3F receptor clustering and spine retraction, through binding to the actin adaptor AnkB and microtubule binding protein DCLK1. I have delineated intracellular binding partners of NrCAM in synapse-enriched cellular fractions. I made a mutation in NrCAM that disrupts binding to AnkB and DCLK1 and perturbs Sema3F holoreceptor functioning. I demonstrated that chemical disruption of microtubules affects spine morphology and response to Sema3F. Finally, I have shown *in vivo* mutations affecting AnkB result in altered spine densities. The findings provide insight toward understanding the molecular mechanisms of dendritic spine remodeling and the pathology of neurodevelopmental disorders involving dendritic spine anomalies.

To my parents, Linda and David Wyatt, for their love and support, and to all of my friends for their kind words along the way. Thank you, I couldn't have done this without you.

ACKNOWLEDGMENTS

This project would not have been possible without the support of many people. First and foremost, thank you to my advisor Patricia Maness, who consistently provided guidance and mentorship, and encouraged out of the box thinking. I have been fortunate to have a supportive and helpful thesis committee, composed of Richard Cheney, Stephanie Gupton, Damaris Lorenzo, and Kathryn Reissner. In addition to group meetings, they have all provided individualized mentorship when I needed it most. I am lucky to have worked with excellent laboratory group members. Postdocs Vishwa Mohan and Chelsea Sullivan were instrumental in experimental design, troubleshooting, and data analysis. Our technicians Alex Kampov-Polevoi and Rebekah Stewart put in long hours working with mice and genotyping, and keeping buffers freshly stocked. Many thanks to our undergraduate researcher, Sarah Wade, for her help counting thousands of dendritic spines and for performing Sholl analysis. Thanks to my significant other, Cedar Mitchell, for her advice, companionship, and most importantly, a listening ear and shoulder to lean on. And last but not least, thanks to my dear friends for their thoughts, edits, and always keeping my spirits lifted, especially LJM and NEB.

TABLE OF CONTENTS

LIST OF FIGURES

LIST OF ABBREVIATIONS

AAV	adenoassociated virus
AnkB	Ankyrin B
AnkB +/+	wild type Ankyrin B
AnkB F/F	Ankyrin B containing LoxP sites flanking exon 24 in the gene sequence
ANOVA	analysis of variance
AP	alkaline phosphatase
AT	axon terminal
ASD	autism spectrum disorder
BCA	bicinchoninic acid
C-4-S	chondroitin-4-sulfate
$CaCl_2$	calcium chloride
CAM	cell adhesion molecule
cDNA	complementary deoxyribonucleic acid
chABC	Chondroitinase ABC
cKO	conditional knockout
CO_2	carbon Dioxide
coIP	coimmunoprecipitation
CRD	cysteine-rich-domain
CSPG	chondroitin sulfate proteoglycan
Cys	cysteine
DCLK1	Doublecortin-Like Kinase 1
DIV	days *in vitro*

DMEM	Dulbecco's Minimal Essential Media
DMSO	dimethyl sulfoxide
E	glutamate
EC	extracellular domain
ECL	enhanced chemiluminescence
EDTA	Ethylenediaminetetraacetic acid
EGTA	Ethylene glycol-bis(β-aminoethyl ether)-N,N,N′,N′-tetraacetic acid
EGFP	enhanced green fluorescent protein
ELISA	enzyme-linked immunosorbent assay
EphA3	ephrin tyrosine kinase receptor A3
ERT2	estrogen-receptor transporter 2
Fc	antibody fragment crystallizable region
Fig	figure
FN	fibronectin
g	Earth's gravity, 9.8 m/s^2
GABA	gamma-aminobutyric acid
GAD	glutamate decarboxylase
GAG	glycosaminoglycans
GAP	GTPase activating protein
GAPDH	glyceraldehyde 3-phosphate dehydrogenase
GEF	guanine exchange factor
GFP	green fluorescent protein
Glu	glutamate

GTPase	guanosine triphosphate hydrolase
H	histidine
h	hours
H_2O_2	hydrogen peroxide
HBSS	Hanks buffered saline solution
HEK293T	Human Embryonic Kidney cell line clone 293T
HEPES	4-(2-hydroxyethyl)-1-piperazineethanesulfonic acid
His	histidine
HRP	horseradish peroxidase
HSPG	heparin sulfate proteoglycan
IACUC	Institutional Animal Care and Use Committee
IB	immunoblot
Ig	immunoglobulin
IgG	immunoglobulin G
IP	immunoprecipitation
IRES	internal ribosomal entry site
K	lysine
Kd	equilibrium disassociation constant
kDa	kilodaltons
LBD	ligand binding domain
LSM	Laser scanning microscope
MB	maleate buffer
MFC	medial frontal cortex

$MgSO_4$	magnesium sulfate
min	minute
mL	milliliter
mM	millimolar
mTOR	mechanistic target of rapamycin
n	number of samples/mice
NA	numerical aperture
NaBH4	sodium borohydride
NaCl	sodium chloride
NaF	sodium fluoride
$NaHCO_3$	sodium bicarbonate
Na_3VO_4	sodium orthovanadate
NCAM	neural cell adhesion molecule
NCAN	Neurocan
NIH	National Institutes of Health
NOC	nocodazole
nm	nanometer
nM	nanomolar
NMDA	N-methyl-D-aspartate
NP-40	nonidet P-40
Npn2	Neuropilin 2
NrCAM	neuron-glia related cell adhesion molecule
Obj	objective

PAC	paclitaxel
PAGE	polyacrylamide gel electrophoresis
PBS	phosphate buffered saline
PFA	paraformaldehyde
PFC	pre-frontal cortex
PlexA3	Plexin A3
PNN	perineuronal net
PSA	polysialic acid
PSD95	post-synaptic density protein 95
PV	parvalbumin
R	arginine
RIPA	radioimmunoprecipitation assays
SDS	sodium dodecyl sulfate
SEM	standard error of the mean
Sema3A	Semaphorin 3A
Sema3F	Semaphorin 3F
SN	synaptoneurosome
TBS	tris-buffered saline
TBST	tris-buffered saline with tween
Tyr	tyrosine
U	units
µm	micrometer
µM	micromolar

V1	primary visual cortex
WFA	*Wisteria floribunda* agglutinin
WT	wild type
Y	tyrosine

CHAPTER ONE: INTRACELLULAR INTERACTIONS OF NrCAM REQUIRED FOR SEMAPHORIN-3F INDUCED SPINE RETRACTION

Introduction

The refinement of neuronal connectivity during adolescence is an important milestone of human development. For information to be efficiently transmitted locally within a region and distally across the brain, a finely tuned cooperation between excitatory and inhibitory signals (E/I balance) must be acquired. To achieve this, cortical development in the adolescent brain undergoes two distinct phases: an initial overabundance of synapses is formed, composed primarily of excitatory inputs onto dendritic spines, followed by a "remodeling" period of pruning spines to refine connectivity and establish E/I balance.[1–4] This is particularly important within the medial frontal cortex (MFC), where essential circuits regulate social behavior, working memory, and cognition relevant to neurodevelopmental disease. Dysregulation of synaptic connectivity manifests into psychiatric disorders, including autism spectrum disorder (ASD), bipolar disorder, and schizophrenia; yet few of the molecular mechanisms underlying synaptic refinement have been identified. A leading hypothesis in the field is that defective spine pruning results in too great of a spine density within the cortex, causing the hyperexcitability phenotype seen in ASD and other neurodevelopmental disorders. Conversely, overactive spine elimination results in too few spines, a common phenotype seen in schizophrenia.[5] Therefore, determining the molecular mechanisms by which dendritic spines are fated for removal or maturation would not only benefit our understanding of the development of the mammalian nervous system, but also provide vital insights into the pathogenesis of

psychiatric diseases which may be due to aberrant refinement of spines.

One mechanism by which synaptic refinement is known to occur is through repellent signaling by the Semaphorin family of proteins.[6] Semaphorins participate in both local and distal signaling, through their expression as transmembrane isoforms, or by their secretion into the extracellular space (Class 3 Semas).[7] Expression of Semaphorin receptor molecules on the surface of a dendritic spine dictates whether the spine is resistant or destined for elimination. The Maness lab has identified an obligate role for the cell adhesion molecule, Neuron-glial related cell adhesion molecule (NrCAM), within the Semaphorin3F (Sema3F) holoreceptor complex.[8] This heterotrimeric receptor complex consists of NrCAM, Neuropilin 2 (Npn2), and Plexin A3 (PlexA3), which co-cluster upon exposure to Sema3F, causing signal transduction, spine retraction, and elimination of the synapse. Knockout mice lacking NrCAM, Npn2, PlexA3, or Sema3F display excess spines and excitatory synapses on apical but not basal dendrites, and exhibit cortical hyperexcitability.[6,8] Apical dendrites are known to differ from basal dendrites in functional connectivity and integration of inputs.[6,8]

NrCAM is a transmembrane protein with a cytoplasmic domain containing motifs that link to the cytoskeleton. The cytoskeleton within the dendritic spine exhibits a unique feature of being composed almost entirely of filamentous actin (F-actin), in contrast to the dendritic shaft, which relies on microtubules for branching and structural rigidity.[9,10,11] L1, a close relative of NrCAM, binds the actin adaptor proteins Ankyrin B (AnkB) and Ankyrin G (AnkG) important for axon guidance. This interaction is shown to be dependent on tyrosine dephosphorylation in the “FIGQY” motif of the L1 cytoplasmic tail.[12] Phosphorylation of the tyrosine residue in FIGQY of L1 by EphB2 disrupts the ankyrin interaction. Analysis of microexons in autistic patients revealed a misregulated protein-interaction network consisting of AnkB and NrCAM,[13]

and 12 human genetic reports identify AnkB (*Ank2*) as a high confidence autism risk factor in the SFARI gene database.[14–17] However, little is known about the role for neuronal AnkB during postnatal brain development because germline knockout of AnkB is 90% lethal by postnatal day P2, and 100% lethal by P21.[18] Thus, it is of critical importance to utilize a novel approach to identify a role for AnkB in dendritic spine development. To do this, I have generated the first conditional, inducible AnkB knockout mouse with an EGFP reporter (Nex1Cre-ERT2: $AnkB^{loxP}$: $EGFP^{loxP}$), in which AnkB can be deleted in cortical pyramidal neurons at specific time points throughout development. Using this tool, I have identified an *in vivo* dendritic spine phenotype due to AnkB deletion at postnatal and adult stages, revealing an importance for this protein in refining synaptic connectivity.

An important goal is to define at the molecular level the binding partners of the NrCAM cytoplasmic tail, that contribute to the functional Sema3F holoreceptor complex. Previous work has shown that when the consensus FIGQY motif is phosphorylated on tyrosine, the L1CAM family member Neurofascin dissociates from Ankyrin[12,] and binds the lisencephaly protein Doublecortin (DCX).[19] NrCAM was shown not to bind DCX,[19] however, I show here that NrCAM binds a DCX homolog, Doublecortin-like Kinase 1 (DCLK1). DCLK1 is a microtubule-binding protein with serine/threonine kinase activity, important for microtubule bundling and linkage to F-actin.[20,21] Like NrCAM, DCLK1 has been shown to constrain spine density and regulate spine morphology (an indication of mature vs. immature spines).[22] Thus, I hypothesized that direct interactions of NrCAM with the dendritic cytoskeleton through AnkB and DCLK1 is required for Sema3F-holoreceptor functioning, and that tyrosine phosphorylation of NrCAM FIGQY acts as a molecular switch for binding of AnkB to regulate sensitivity to Sema3F-induced spine retraction.

It is of crucial significance to improve our knowledge of how the developing brain determines which connections to keep and which ones to eliminate, to produce a healthy functioning central nervous system. Because glutamatergic inputs onto dendritic spines represent >90% of the connections in the brain, the regulation of spine fate presents the most likely avenue for understanding this process. The Sema3F-mediated elimination signals outlined here provide a robust mechanism for signaling for spine retraction. Other emerging regulators of spine elimination involve astrocyte-mediated engulfment of spines,[23] microglial phagocytosis,[24,25] and autophagic recycling through mTOR signaling.[26,27] The experiments performed in this project are expected to contribute to our understanding of the developmental spine refinement period. The data shown can likely be extended towards understanding how other repellent ligands (Semaphorins 4-7, Ephrins) regulate synapses to achieve appropriate E/I balance in cortical circuits.

MATERIALS AND METHODS

Mice

Wild type (WT) mice were on a C57Bl/6 background from Jackson Laboratories. NrCAM-null (gift from Dr. Martin Grumet), were originally on a mixed background of 129S6/EvSvTac and Swiss Webster, but were subsequently bred into a C57Bl/6 background. L1Y^{1229}H mutant mice are on a C57Bl/6 background. Because the L1 gene is on the X chromosome, heterozygous females were crossed with C57Bl/6 WT males to obtain WT and hemizygous male mutants for analyses (homozygous mutation in females resulted in embryonic lethality). Ankyrin B floxed mice[28] were crossed to the *NexCre-ERT2* line[29] to induce recombination in postmitotic, postmigratory pyramidal neurons upon induction by treatment with tamoxifen, as described.[29] Induction of CreERT2 in a sparse population of cells was performed through daily intraperitoneal administration of 4-hydroxy-tamoxifen from P10 to P13, and mice were analyzed at P28 or P50. The Rosa-CAG-EGFP (RCE, gift from Gordon Fischell) reporter mouse line was crossed to the *NexCRE-ERT2* mice prior to breeding with Ankyrin B floxed mice. It contains a loxP-stop-LoxP EGFP allele for specific labeling of Cre-induced cells.

Immunoreagents and chemicals

Monoclonal antibodies used were directed against NrCAM (Abcam, ab24344), ankyrin B (Thermo Fisher, 33-3700), DCLK1 (Abcam, ab31704), spinophilin (Millipore, 06-852) phospho-FIGQY (Bethel Laboratories, made on-demand). Polyclonal antibodies were: Npn-2 (R&D Systems, AF567), PlexA3 (Abcam, ab41564), EGFP (Abcam, ab13970). Normal rabbit IgG was obtained from Jackson Immunoresearch. Horseradish peroxidase, Alexafluor488, Alexafluor555, and Alexafluor647-conjugated secondary antibodies were obtained from Jackson Immunoresearch. For western blotting all antibodies were diluted in 5% milk/TBST. Primary

antibodies were used at a 1:1000 dilution from stock, HRP anti-mouse 1:5000, and HRP anti-rabbit 1:10,000. For immunostaining, primary antibodies were used at 1:500 dilution in 5% donkey serum/PBS, and AlexaFluor 488, 555, and 647 secondary antibodies were used at 1:500 dilution in PBS. Fc fragment from human IgG was from Abcam, and Sema3F-Fc fusion protein was from R&D systems. Microtubule perturbing compounds taxol and nocodazole were purchased from Sigma Aldrich. 4-hydroxy-tamoxifen for induction of NexCre-ERT2 was purchased in freebase form from Sigma (T5648) and dissolved in sunflower oil (Sigma, S5007).

HEK293T cell culture and transient transfection

HEK293T cells were grown in DMEM supplemented with gentamicin/kanamycin (Sigma) and 10% FBS (Gibco) in a humidified incubator with 5% CO_2. On the day before transfections, cells were seeded at $1x10^6$ cells per 100mm dish. Plasmids containing WT or mutant NrCAM were cotransfected with either Ankyrin B or DCLK1 at a 2:1 molar ratio with Lipofectamine 2000 (ThermoFisher, 11668) following manufacturer protocol. Media was changed on the day following transfection, and cells harvested 48 h later in RIPA (20 mM Tris, pH 7.0, 0.15 M NaCl, 5mM EDTA, 1 mM EGTA, 1% NP-40, 1% deoxycholate, 0.1% SDS, 200 µM Na_3VO_4, 10 mM NaF, 1x Protease Inhibitor Cocktail (Sigma)) or Triton (20 mM Tris, pH 7.0, 150mM NaCl, 5 mM EDTA, 1 mM EGTA, 1% TritonX100, 10 mM NaF, 1x Protease Inhibitor Cocktail (Sigma)). Protein concentrations were determined using BCA.

Synaptoneurosome Preparation

Synaptoneurosomes were isolated as in Villasana et al.[30] Adolescent aged wild type mice were anesthetized, decapitated, and the cortex isolated (n = 4 brains per SN prep) then dounce homogenized in synaptoneurosome buffer containing additives (10 mM HEPES, 1 mM EDTA, 2 mM EGTA, 10 mM NaF, 1x Protease Inhibitor Cocktail (Sigma)) for 20 strokes on ice.

Homogenate was briefly sonicated 6x for 10 seconds each with 60 seconds of rest on ice between each cycle, then filtered 3x through a 100 µm nylon filter followed by 1x through a 5 µm cell strainer. The final filtrate was centrifuged at 1000 x *g* for 10 minutes at 4 ºC. The pellet was resuspended in 500 µL of TRITON lysis buffer containing additives, nutated on a rocker for 40 minutes at 4 ºC, then centrifuged at 16,000 x *g* on a table top centrifuge for 10 minutes at 4 ºC. The supernatant was collected as a the synaptoneurosome fraction, protein concentration determined using BCA, and PSD95 enrichment verified through SDS-PAGE and western blotting.

Immunoprecipitation

Mouse forebrain lysates were extracted and dounce homogenized for 20 strokes in RIPA. Homogenate was incubated for 15 minutes on ice, then centrifuged at 16,000 x *g* for 10 minutes. The supernatant was retained and protein concentration determined through BCA. Forebrain lysates (1 mg) or HEK293T cell lysates (0.5 mg) were precleared for 30 minutes at 4 ºC using Protein A/G Sepharose beads (ThermoFisher). Precleared lysates were incubated with 3 µg of NrCAM or nonimmune rabbit IgG antibodies for 2 h on ice. Fresh Protein A/G sepharose beads were added for an additional 30 min with nutation at 4 ºC before washing with RIPA or TRITON. Beads were washed 4x, then immunoprecipitated proteins were released from the beads by boiling in SDS-PAGE sample buffer (125 mM Tris pH 6.8, 4% SDS, 20% glycerol, 10% β-mercaptoethanol, 2 mM EDTA, 0.005% bromophenol blue).

Cortical neuron culture

Cortical neurons were prepared from brains of WT or NrCAM-null embryos (E15.5) and transfected with pCAGG-IRES-mEGFP (empty vector), pCAGG-IRES-NrCAM-EGFP (WT NrCAM), or pCAGG-IRES-FIGQH-EGFP (Y1231H mutant), as described.[6,8] Media was

changed every 48-72 hours until DIV 14. At DIV 14, cultures were treated with DMSO (0.5%), Taxol (100 nM), or Nocodazole (7 µM) for 4 hours, or Sema3F-Fc and Fc control protein (3 nM) for 30 minutes. Cultures were fixed with 4% PFA for 20 min, permeablized with 0.3% TritonX100 for 30 min, blocked with 10% donkey serum for 1 h, and stained with primary antibodies (1:500) overnight. AlexaFluor488, 555, or 647 secondary antibodies (1:500) were incubated for 1h the next day. Images were captured on a LSM700 confocal microscope with 20x/0.8 NA Plan Apo lens for whole neuron images, or a 40x/1.4 NA Plan Apo oil immersion lens with 2.5x optical zoom for dendritic spine images. Spines of labeled neurons were measured on dendrites of at least 10 neurons in each of four replicate cultures per condition. Mean spine densities ± SEM were determined for each condition and compared by two tailed *t* test ($p < 0.05$). For co-localization analysis, EGFP was used to label neurons, and proteins of interest labeled with AF555 and AF647.[31] ImageJ Coloc2 plugin was used to quantify colocalized pixels and represented by thresholded Mander's coefficient and Pearson's Coefficient, and means ± SEM compared by two tailed *t* test ($p < 0.05$).

Spine density and Sholl analysis of Golgi-impregnated neurons

Mice (P60) were anesthetized with isofluorane and brains were removed and processed for Golgi staining using the FD Rapid GolgiStain Kit (FD NeuroTechnologies, PK 401). Brains were embedded in Golgi solutions A & B for 3 weeks, then flash frozen in isopentane pre-chilled on dry ice. Frozen brains were cryostat sectioned (100 µm coronal) and mounted on gelatin-coated microscope slides for histochemical staining according to manufacturer protocol. Golgi-labeled neurons were analyzed in coronal sections of mouse brain using an Olympus BX-61 microscope with z-stack capabilities, and images captured with a 20x objective for Sholl analysis and 63x objective for spine analysis. Spine density and dendritic branching were quantified using

Neurolucida software (MBF Bioscience). For apical dendrites, spines were scored along the primary segment 100-150 µm distal to the soma. For basal dendrites, spines were scored along 35-50 µm segments on 3-5 secondary branches. Mean spine number per 10 microns of dendrite (density) was calculated. For Sholl analysis, the center of concentric circles was defined as the center of the cell body, and then dendritic arbors traced manually, with a starting radius of 10 µm and radius increments of 10 µm ending at 300 µm.

RESULTS

NrCAM interactions at the synapse and dependence on Tyr1231

To evaluate a role for an interaction between the cytoplasmic tail of NrCAM with the cytoskeleton of dendritic spines, a series of co-immunoprecipitation binding assays were performed in lysates collected from synaptoneurosome fractions of wild type brain tissue, and whole protein lysates from HEK293T cells transfected with cDNAs for proteins of interest. NrCAM was found to immunoprecipitate with both AnkB and DCLK1 from synaptoneurosomes (Fig 1A), which are fractionated pre- and post-synapse compartments collected from whole mouse cortex. DCLK1-interacting protein Spinophilin, and the guanine nucleotide exchange factor Tiam1 were also shown to immunoprecipitate with NrCAM (Fig 1A). High magnification confocal imaging of wild type cortical neurons labeled with EGFP and immunostained for NrCAM and AnkB reveal co-localization of these two proteins within the dendritic spine (Fig 1B). To determine whether these proteins directly bind NrCAM or indirectly associate through a complex, I expressed each protein in isolation with NrCAM using Lipofectamine2000 co-transfection of cDNAs into HEK293T cells. Interestingly, only AnkB and DCLK1 were shown to bind NrCAM in this system (Fig 1B,C). Co-transfection of NrCAM with Tiam1 cDNA did not yield any Tiam1 pulled down when expressed in isolation (Data not shown). Furthermore, coexpression of AnkB with DCLK1 in HEK293T cells revealed no direct binding, suggesting these proteins bind to NrCAM independently of each other (Fig 1D).

To further explore the binding of AnkB and DCLK1 to NrCAM, I generated a tyrosine-1231 to histidine point mutation in the putative AnkB binding site on the cytoplasmic tail of NrCAM, termed Y1231H, and co-expressed this cDNA in HEK293T cells with AnkB or DCLK1. I found that the NrCAM/DCLK1 association was completely eliminated, and the

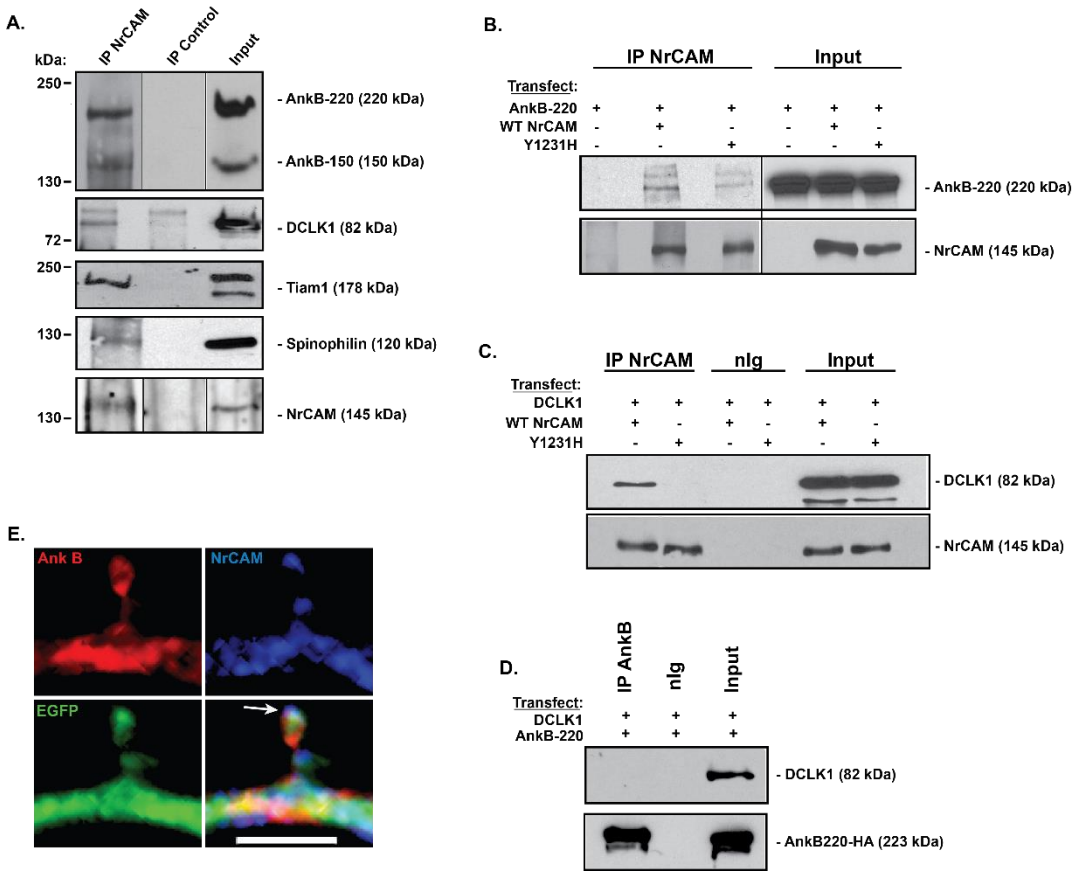

Figure 1. Intracellular interactions of NrCAM at the synapse. (A) Synaptic subcellular fractions, "synaptoneurosomes," were isolated from p28 mouse forebrain, NrCAM co-immunoprecipitated, and immunoblotted for intracellular binding partners. (B) HEK293T cells transfected with cDNAs for AnkB220-HA +/- WT NrCAM or Y1231H mutant show reduced binding in Y1231H. AnkB220-HA transfection in the absence of NrCAM was treated as negative control. (C) HEK293T cells transfected with DCLK1 +/- WT NrCAM or Y1231H mutant and co-immunoprecipitated for NrCAM. (D) HEK293T cells transfected with AnkB220-HA and DCLK1 cDNAs, and co-immunoprecipitated for AnkB demonstrate no binding interaction. (E) High resolution confocal imaging of wild type neuron labeled with EGFP and immunostained for AnkB (red) and NrCAM (blue) show colocalized pixels within the head of dendritic spines (white arrow). Scale bar = 3 µm.

NrCAM/AnkB interaction was significantly reduced (Figure 1B). This mutation is homologous to the L1 syndrome Y1229H mutation in the L1 cell adhesion molecule, a close relative of NrCAM.

Y1231H mutation in cytoskeletal binding site disrupts Sema3F-induced spine retraction and Npn2/PlexA3 clustering

Because NrCAM has been previously identified as a critical mediator for the repellent function of the secreted Semaphorin3F ligand,[8] I wanted to explore whether the loss of binding to the AnkB and DCLK1 cytoskeletal interactors would affect the ability of Sema3F to initiate

spine retraction. To do this, I designed a rescue experiment using Lipofectamine2000 transfection of NrCAM cDNAs into cortical neuron cultures generated from NrCAM-*null* mice, and then treated these neurons with recombinant Sema3F-Fc or Fc control for 30 minutes. These neurons were labeled by an EGFP reporter on the cDNA vector to identify which neurons received the rescue construct (Fig 2A). Spine density was assessed on apical dendrites of pyramidal neurons, 100-150 µm from the soma, because our lab previously identified that Sema3F spine retraction signaling only effects apical dendrites and not basal. As a control, empty pCAGGS-IRES-EGFP vector was transfected and shown to have no effect on rescuing the spine retraction phenotype typical of Sema3F-Fc treatment, while transfection of WT NrCAM plasmid resulted a 33% reduction in mean spine density, represented as spines per 10 µm of dendrite. Rescue with the Y1231H NrCAM was unable to rescue the Sema3F spine retraction phenotype (Fig 2A,B).

Our lab has previously shown that treatment of neuron cultures from wild type mice causes clustering of Npn2 and PlexA3, subunits of the Sema3F holoreceptor complex, as indicated by their increased co-localization in immunostaining along dendrites.[31] I used this model to explore the putative mechanism for the loss of spine retraction in NrCAM-*null* neurons rescued with Y1231H. Neurons were cultured from NrCAM-*null* neurons, transfected with WT or Y1231H pCAGGS-IRES-EGFP plasmids, and surface stained for extracellular Npn2 and PlexA3 (Fig 2C). Confocal imaging and ImageJ colocalization software were used for analysis. Baseline co-localization across all transfection conditions treated with recombinant Fc protein, demonstrated by a mean Pearson's P value between 0.25-0.35 (Fig 2D) and mean thresholded Mander's tM1 and tM2 coefficients from 0.40-0.55 (Fig 2E,F) were low. Following 30 min treatment with Sema3F-Fc, the intensity of co-localized Npn2/PlexA3

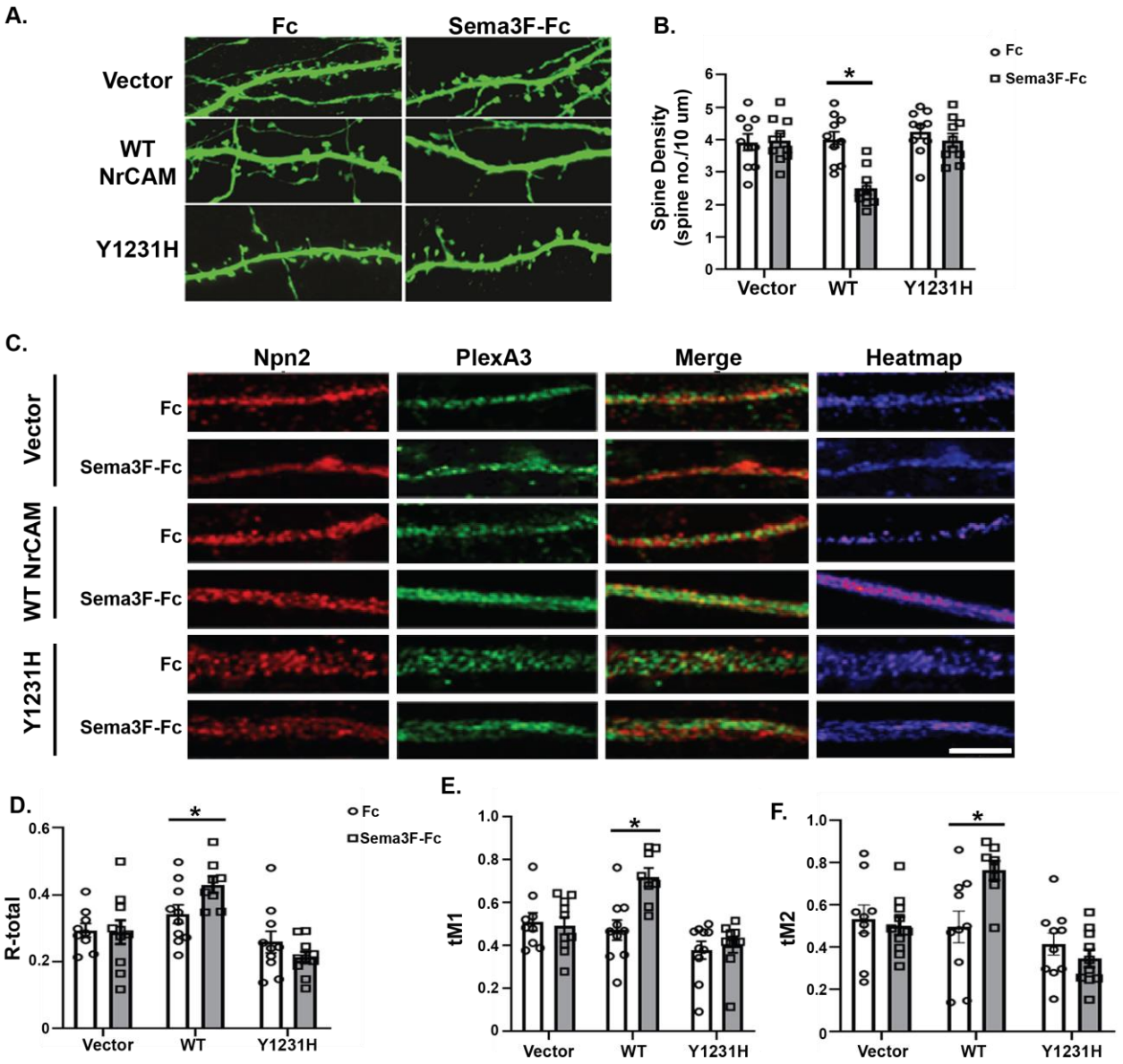

Figure 2. Y1231H mutation disrupts Sema3F holoreceptor functioning. NrCAM-null neurons were transfected with EGFP vector, WT NrCAM, or Y1231H mutant in pCAGG-IRES-mEGFP, treated with Fc or Sema3F-Fc for 30 minutes on DIV14, immunostained for EGFP, and apical dendrites imaged confocally. (B) Quantification of mean spine density ± SEM on apical dendrites (n > 10 neurons per condition, t test, *P < 0.05). (C) Confocal images of apical dendrites of NrCAM-null neurons transfected as described in (A), treated with Fc or Sema3F-Fc for 30 minutes, and stained for Npn2 (red) and PlexA3 (green). Merged images and heat maps of colocalization are shown. Scale bar = 5 µm. (D) Bar graph of Pearson's R-total coefficient evaluating degree of colocalization and colocalized pixel intensity (n = 3 replicates, 10 neurons/replicate/condition, *P < 0.05). (E,F) Thresholded Mander's coefficients demonstrating degree of pixel colocalization, in (E) Npn2 vs PlexA3, in (F) PlexA3 vs Npn2 (n = 3 replicates, 10 neurons/replicate/condition, *P < 0.05). Open circles represent Fc-treated neurons, open squares represent Sema3F-Fc treatment.

pixels increased to 150% of baseline across all statistical measures for WT NrCAM rescue neurons compared to Fc controls, but no difference was seen for NrCAM-*null* and His1231-

expressing neurons (Figs 2D,E,F).

Chemical disruption of microtubules significantly impairs dendritic spine health and functioning

The requirement for Tyr1231 residue for binding of NrCAM and the microtubule-binding protein DCLK1, and the loss of Sema3F-induced spine retraction due to this mutation suggests a potential role for microtubules in the spine retraction mechanism. To pursue this hypothesis, I treated wild type cortical neuron cultures with the microtubule stabilizing compound Paclitaxel (10 nM, 4 hours) and the microtubule destabilizing compound Nocodazole (7 µM, 4 hours), and measured the efficacy of Sema3F-Fc treatment on spine density. Low magnification confocal imaging revealed an abundance of filopodial protrusions on nocodazole treated neurons (Fig 3A), suggesting a requirement of microtubules in constraining spinogenesis. Confocal analysis of the dendritic spines of apical dendrites (Fig 3B) revealed a significant impairment of Sema3F-Fc induced spine retraction when microtubule function is disrupted, whereas 0.1% DMSO vehicle controls were unaffected (45% reduction in spine density for DMSO control, 13% reduction in paclitaxel treated neurons, and 3% reduction in nocodazole treated neurons, ± SEM). There was lowered baseline level of spine density in the Fc-treated control groups of 12% and 21% for paclitaxel and nocodazole treated groups, respectively.

Dendritic spines in culture can be found in both their immature and mature states, based on morphological characteristics. An observation was made during confocal imaging that the nocodazole treated neurons displayed significantly more immature filopodial spines than controls. Further analysis of the ratio of immature to mature spines in each condition was conducted and revealed a 58% to 42% ratio of immature to mature dendritic spines in the Fc-treated DMSO control neurons, however in the PAC and NOC-treated neurons there were significantly more immature spines in Fc-treated controls with mean ratio of 78% to 22.2% and

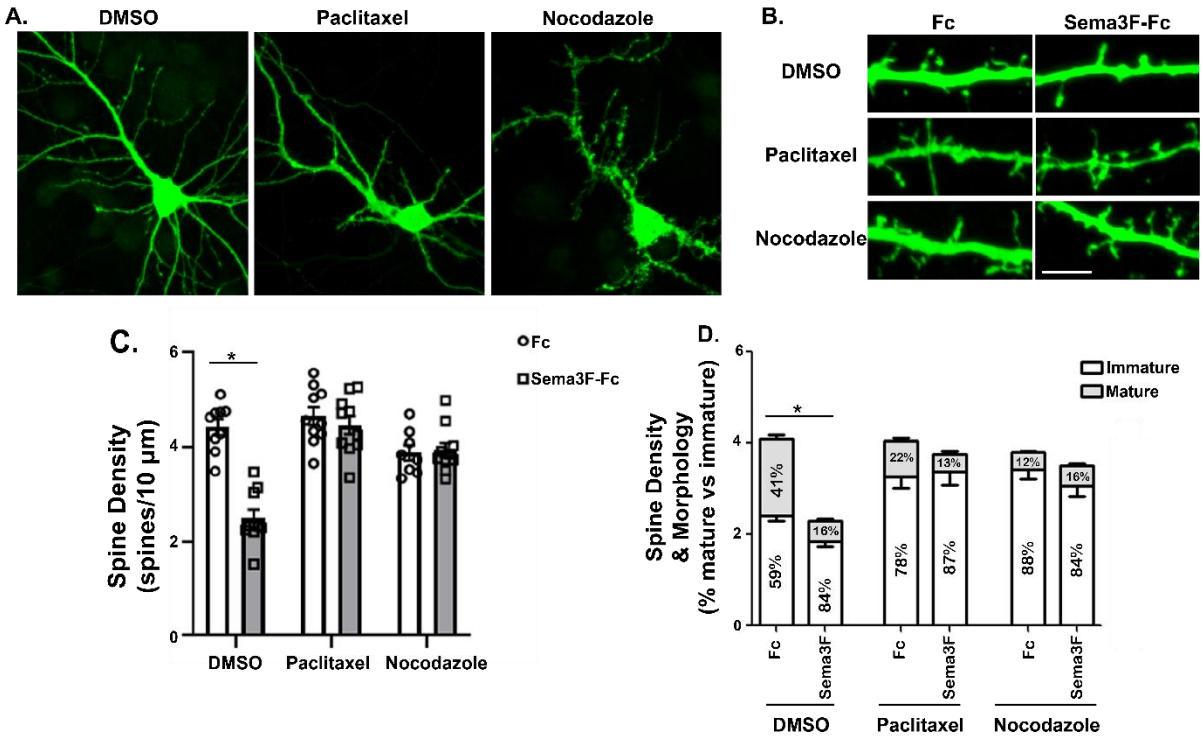

Figure 3. Chemical disruption of microtubules impairs spine development and retraction. (A) Wild type neuron cultures were transfected with pCAGG-IRES-mEGFP vector, and treated with 100 nM paclitaxel or 7 µM nocodazole for 4 hours prior to treatment with 3 nM Fc or Sema3F-Fc. Whole neurons were imaged using confocal microscopy (20x objective, 0.8 NA) to assess cellular morphology. (B) High magnification images (40x obj, 1.4 NA, 2.5x optical zoom) of apical dendrites from neurons described in A. (C, D) Quantification of dendritic spine density (mean spine density ± SEM, n = 3 replicates, 10 neurons/replicate/condition, t-test, *P < 0.05) and morphologies (mean ratios ± SEM, two-way ANOVA, *P < 0.05)

88% to 12%, respectively (mean ratios ± SEM, two-way ANOVA). Across all treatment conditions, there was approximately a 6:1 ratio of immature:mature spines following 30 minute Sema3F-Fc treatment, demonstrating that mature spines are preferentially lost upon Sema3F holoreceptor activation.

Y1229H mutation in L1 cell adhesion molecule affects spine density *in vivo*

The Tyr to His mutation in the conserved cytoplasmic FIGQY binding site of L1-CAM family members has been identified as a risk factor for the human L1 syndrome neurodevelopmental disorder. Our lab previously identified a loss of binding between Ankyrins and L1 in a mouse model containing this mutation. To determine a molecular phenotype for the Tyr-His mutation in an existing *in vivo* mouse model, I performed Golgi-Cox

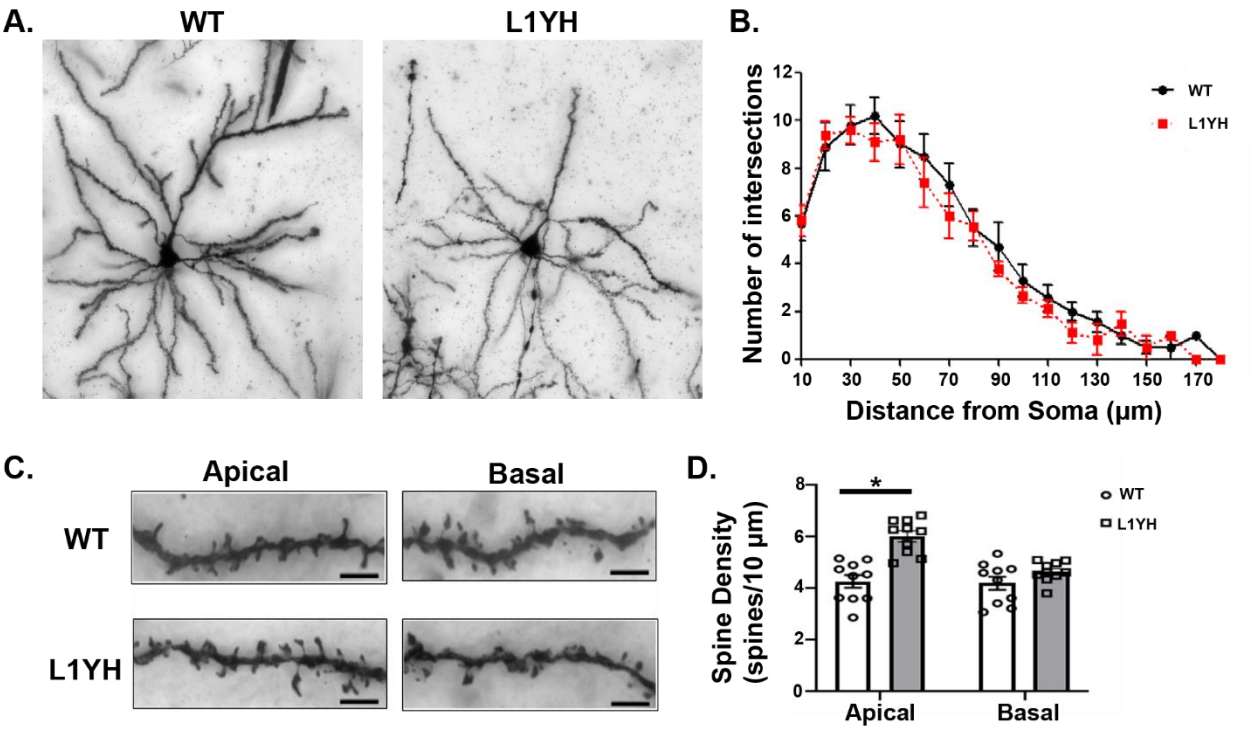

Figure 4. L1YH mutation increases spine density on apical dendrites but has no effect on dendritic branching. (A) Representative golgi-labeled pyramidal neurons in MFC of P60 adult mice. (B) Sholl analysis of dendrite arborization quantified in 10 µm increments from the cell soma, means ± SEM (3 mice, n = 10 neurons/mouse). (C) Representative Golgi-labeled apical dendrites from WT and L1YH P60 adult mice, scale bar = 5 µm). (D) Quantification of mean spine density ± SEM from golgi-labeled apical dendrites as shown in C (n = 3 mice/genotype, 10 neurons/mouse, *P < 0.05)

staining of mouse brains containing the Y1229H mutation in the L1 gene, a close family member of NrCAM. Coronal sections were taken from the medial frontal cortex (MFC) of L1YH mice sacrificed at postnatal day P60, when the remodeling of spine density during adolescence has been completed. Low magnification wide field light microscopy images (20x objective/0.5 NA, 1 µM z-series sections) were captured to analyze whole-cell dendrite arborization. Sholl analysis revealed no significant difference between the number of branch intersections up to 170 µm away from the soma, stratified by 10 µm increments (Fig 4A**)**. High magnification (60x Obj, 1.42 NA) images were captured to quantify spine densities. Concurrent with previous findings for NrCAM-*null* dendrites, it was found that basal dendrite spine density was unaffected by the L1YH mutation (WT: 4 spines/10 µm, L1YH: 4 spines/10 µm, mean ± SEM), however apical

dendrite spine density was significantly increased in the L1YH mice by 27% (WT: 4 spines/10 µm, L1YH: 6 spines/10 µm, means ± SEM), as shown in Figure 4b.

Postnatal deletion of Ankyrin B in pyramidal neurons disrupts regulation of spine density

To overcome the early postnatal lethality of germline AnkB deletion, and to explore the consequence of postnatal deletion specifically in pyramidal neurons, I generated a conditional inducible knockout line. Daily tamoxifen induction of cre recombinase under the *Nex1* promoter from P10-P13 led to a decreased intensity of AnkB fluorescence in the medial frontal cortex at P28 as seen through immunostaining and confocal microscopy (Fig 5A). Background AnkB signal in the cKO tissue is due to non-*Nex1*-expressing neurons and glial cells which did not undergo cre recombination. EGFP+ neuronal processes can be seen more readily in the AnkB deficient tissue, whereas in the Nex1Cre/RCE control mice, AnkB fluorescence overshadows most EGFP signal except for the cell soma. The tamoxifen-specific induction of cre activity was validated by immunostaining for EGFP in tamoxifen treated tissue and compared to non-injected controls. No EGFP signal is seen in the non-injected controls, compared to the desired mosaic labeling in tamoxifen injected brain tissue. The cKO mice displayed no major abnormalities in cortical thickness, corpus callosum and anterior commissure thickness, and apparent volume of the third vesicle (Fig 5C). To explore the *in vivo* role for AnkB in dendritic spine remodeling, high resolution (63x obj/1.42 NA) confocal images were taken of EGFP+ apical dendrites in the medial frontal cortex of AnkB F/F and AnkB +/+ Nex1Cre:RCE mice injected with tamoxifen from P10-P13, and harvested at P28 (mid-adolescent) or P50 (young adult). No difference in mean spine density was seen between genotypes at P28 (AnkB +/+: 5 spines/10 µm, AnkB F/F: 5 spines/10 µm, ± SEM), however, there was a 31% increase in mean apical spine density at P50 (AnkB +/+: 6 spines/10 µm, AnkB F/F: 9 spines/10 µm, ± SEM) shown in figure 5D,E.

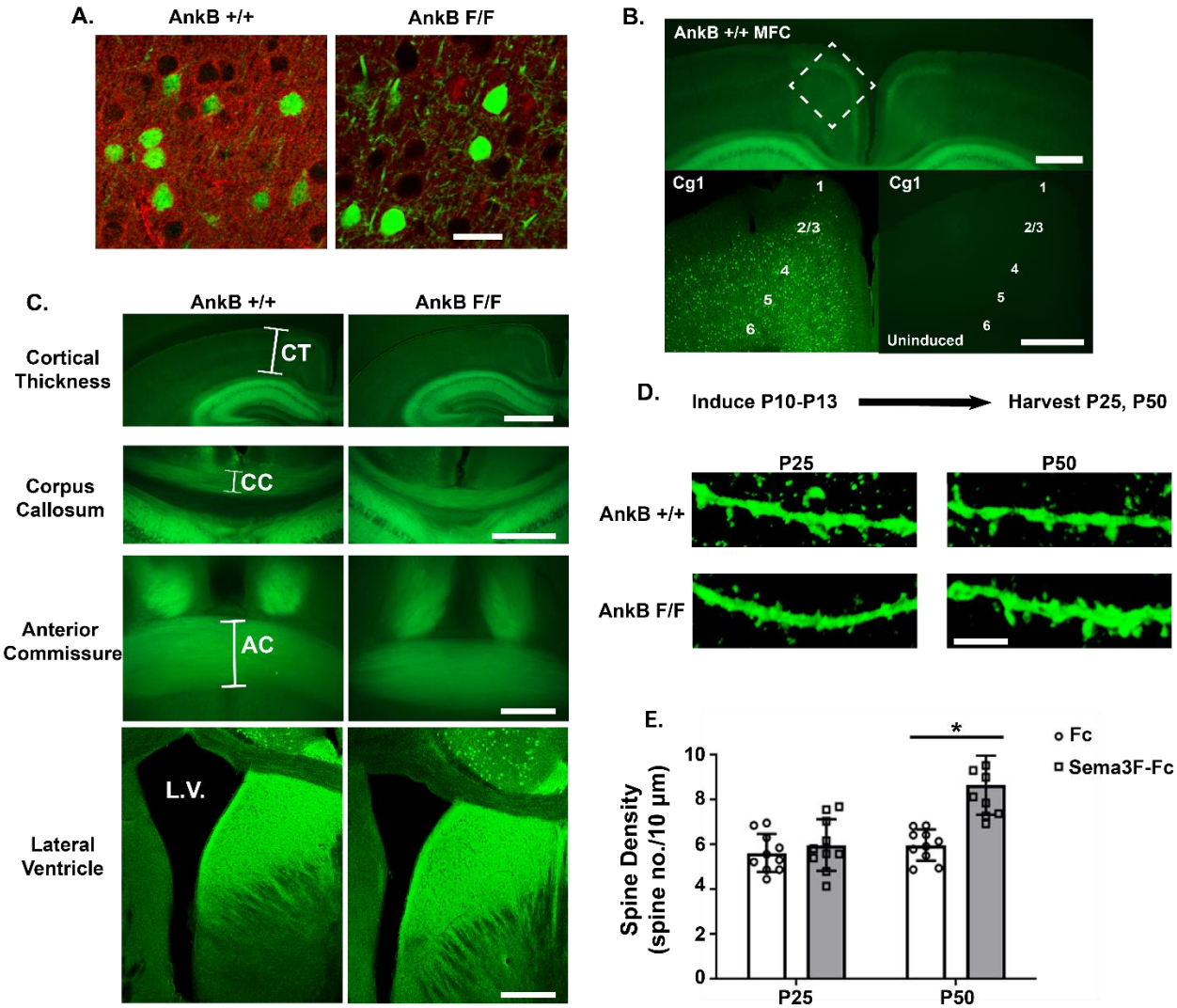

Figure 5. Conditional deletion of Ankyrin B in postnatal, post-mitotic pyramidal neurons. (A) Reduced immunostaining of AnkB (red) in MFC of P10-P13 tamoxifen injected mice labeled with EGFP reporter in cells with Nex1Cre recombination compared to AnkB +/+ (WT alleles). Scale bar = 50 µm. (B) EGFP labeling of MFC neurons following induction as in A. White box bounds cg1 cingulate cortex, zoomed in bottom left panel. Bottom right panel shows no labeling in uninduced controls, labeled for cortical layers. (C) Major neuroanatomical features showing cortical thickness (CT), anterior commissure (AC) and corpus callosum (CC) axon tracts, and volume of lateral ventricle (L.V.). Scale bar = 100 µm, 50 µm, 25 µm, and 25 µm top-to-bottom. (D) Early postnatal deletion of AnkB has no effect on spine density by early adolescent P21, but causes increased apical spine density by young adult P50. Scale bar = 5 µm. (E) Representative quantification of spines represented in D, means ± SEM, n = 2-3 mice/genotype/age, 10 neurons/mouse. t-test *P < 0.05)

DISCUSSION

The molecular mechanisms governing the regulation of dendritic spine numbers during development remain incompletely understood. One major mechanism is the crosstalk between neurons through the chemorepulsive semaphorin molecules, particularly the secreted class 3 semaphorins, termed Sema3.[6] Previous work has shown a receptor complex for Sema3F on the surface of dendritic spines that consists of NrCAM, Neuropilin2, and PlexA3.[32] The data presented in this chapter demonstrate a critical role for intracellular interactions of the cell adhesion molecule NrCAM to correctly refine cortical dendritic spine density, important for establishing healthy brain connectivity. I showed that NrCAM binds to cytoskeletal interacting proteins Ankyrin B (actin) and DCLK1 (microtubules, signaling) (Fig 1A), and this binding is dependent on Tyr1231 residue in the "FIGQY" motif within the cytoplasmic tail (Fig 1C). Upon Sema3F docking to the holoreceptor complex, there is a structural rearrangement that occurs, termed "clustering," which allows for the release of auto-inhibition of the PlexA3 intrinsic Rap-GAP activity inside the cell.[31] Unpublished data from our lab have demonstrated a potential dual-signaling pathway involving Rac1 signaling, which I hypothesized was achieved initially through activation of the GEF Tiam1. I haveve shown that NrCAM indirectly associates with Tiam1 in synaptoneurosomes (Fig 1A), potentially through a complex of NrCAM-DCLK1-Spinophilin-Tiam1. Binding of NrCAM to DCLK1 is dependent on the Tyr1231 residue, as single amino acid change to histidine completely eliminates binding (Fig 1C). Further research needs to be done to characterize the direct binding of each protein within complex using recombinant proteins *in vitro*.

In addition to a dual-signaling mechanism initiated by NrCAM, I hypothesized that NrCAM binding to the actin cytoskeleton through the spectrin-binding protein Ankyrin B would

provide structural support for the clustering action of the receptor complex. Previous studies have identified AnkB as a high-confidence autism risk factor,[14–17] and an observed phenotype in human autism patients is an elevated density of dendritic spines in the cortex,[7] further supporting our hypothesis. Tyr1229 in the L1 cell adhesion molecule, the homologous tyrosine residue to NrCAM Tyr1231, has been shown to regulate binding of L1 to Ankyrin proteins in developing axons and retinocollicular targeting.[12,33] Phosphorylation of NrCAM Tyr1231 was shown to be developmentally dynamic in mouse brain lysates (Fig 1D), although the tyrosine kinase and phosphatase that regulate the phosphorylation state remain unknown. This led me to the hypothesis that AnkB also interacts with NrCAM, likely through the same residue, as a conserved cytoskeletal binding partner for correct localization of neural cell adhesion molecules on the surface of the cell. Using high resolution confocal microscopy, I have demonstrated for the first time that AnkB is present within the dendritic spine compartment, and co-localizes with NrCAM (Fig 1B). Co-immunoprecipitation of AnkB with NrCAM is significantly reduced with the Y1231H mutation in cDNA (Fig 1C). Furthermore, rescue of NrCAM-*null* neurons with the Y1231H mutant resulted in a resistance to Sema3F-induced spine retraction (Fig 2A,B). There was a loss of holoreceptor clustering following 30 minute Sema3F treatment as demonstrated by triple color immunostaining and confocal microscopy of Y1231H-transfected NrCAM-null neurons (Fig 2C-F).

To characterize this mechanism further it would be informative to create a mouse model containing the point mutation in NrCAM Y1231 and validate the effect *in vivo*. Such a mouse does not yet exist, however, there is an existing mouse line containing the homologous Y to H mutation in L1 Y1229, termed "L1YH." The L1YH mouse was shown to be deficient for Ank binding to L1 and recruitment of Ank to the plasma membrane, which led to an impairment in

axon targeting and retinocollicular mapping in the developing mouse.[33] It was also found that the His1229 L1 mutation led to increased endocytosis of L1, supporting the idea that ankyrins are important for structural localization of cell adhesion molecules to the cell surface. Because the previous studies were focused on axonal effects, I hypothesized that these mutants would also display dendrite phenotypes in the adult cortex, as a result of a malfunctioning adolescent refinement period. To address this question, I performed Golgi-Cox staining of adult (P60) L1YH mouse brains and wild type littermates to directly label neurons without a fluorescent reporter or antibody staining. Whole-cell analysis of pyramidal neuron dendrites in the medial frontal cortex revealed no effect on dendritic arborization as quantified through Sholl analysis (Fig 4A,B). However, strikingly, there was a significant increase in apical spine density in L1YH mutants compared to wild type controls (Fig 4C). Basal spines were not affected. This corroborates the findings in cultured neurons from NrCAM-*null* mice (Fig 2), and further suggests the model of cell adhesion molecule binding to the cytoskeletal components for dendritic refinement. It will be important to continue exploring this system from a biochemical approach, using synaptoneurosome fractionations and cultured neurons *in vitro*.

The binding interaction between NrCAM and DCLK1 is likely to be important for downstream Rac1 signaling through Tiam1. Yet, DCLK1 is an established microtubule binding protein, and recent studies have implicated a role for microtubules in dendritic spine functioning.[10] Whereas before it was thought that spines were isolated structures consisting solely of filamentous and globular actin, this provides an exciting new mechanism for exploring the intracellular mechanisms of the Sema3F holoreceptor. To explore the possibility of microtubule requirement for Sema3F spine retraction, I hypothesized that chemical disruption of microtubule function would result in an impairment of Sema3F-induced spine retraction. Like

actin, microtubules (MT) exist in a dynamic state of treadmilling tubulin monomers which form a microtubule filament. Paclitaxel, a plant alkaloid FDA-approved for cancer chemotherapy, binds to beta-tubulin subunits of microtubules and prevents disassembly of the MTs which blocks the treadmilling required for healthy functioning. Indeed, treatment of wild type culture neurons with 100 nM paclitaxel impaired the ability of Sema3F to induce spine retraction (Fig 4A). A synthetic antineoplastic agent, nocodazole (NOC), also binds to beta-tubulin in MT filaments, but instead of stabilizing the filament, NOC blocks addition of tubulin to the (+) end, leading to disassembly of MTs.[34] In accord with the experiment with PAC, treatment of wild type cultured neurons with 7 µM NOC prior to Sema3F application resulted in a loss of sensitivity to Sema3F (Fig 3A). More experiments are needed to explore if chemical disruption of MTs impairs Npn2/PlexA3 clustering and RapGAP signaling directly, or if the effects seen are further downstream of the receptor complex.

AnkB is a critical actin-associated protein that is expressed in all mammalian tissues, including heart and brain. Germline knockout of AnkB is lethal to 90% of pups by postnatal day two.[18] Furthermore, it is expressed in non-pyramidal neurons in the brain and in glia. To overcome the early postnatal lethality and to explore the consequence of postnatal deletion specifically in pyramidal neurons, I generated a conditional inducible knockout line. AnkB floxed mice were intercrossed to the *Nex1*Cre-ERT2 knock-in mouse line, in which a modified cre recombinase fused to the estrogen receptor transporter ligand binding domain is under control of the *Nex1* gene. Temporal knockout of AnkB is achieved by intraperitoneal injection of 4-hydroxy-tamoxifen (100 mg/kg) to induce nuclear import of the cre recombinase/ERT2 complex from postnatal day P10-P13, during the major spinogenesis period but prior to adolescent spine remodeling. The EGFP-expressing RCE reporter mouse line was also

intercrossed for permanent cell-specific labeling of recombinase activity (Fig 5B), which showed no “leakiness” of recombination in the absence of tamoxifen. Immunohistochemical analysis of AnkB expression in the medial frontal cortex demonstrated reduced AnkB fluorescence in induced AnkB F/F Nex1Cre:RCE mice compared to AnkB +/+ controls (Fig 5A). The background AnkB signal shown is likely due to non-Nex1 expressing neurons as well as glial cells which still produce AnkB. Confocal imaging revealed that postnatal deletion of AnkB specifically in pyramidal neurons had no effect on major neuroanatomical features that are required for healthy neurodevelopment: cortical thickness, integrity of major axon tracts (corpus callosum, anterior commissure), and ventricular volume (Fig 5C). Due to the novelty of this transgenic mouse model, it is important to rule out such impairments prior to exploring impaired cellular mechanisms. Moreover, high magnification confocal microscopy targeting pyramidal neurons in the medial frontal cortex demonstrated an increase in mean spine density of EGFP+ (AnkB-*null*) neurons in the induced AnkB F/F mouse at P50, after the closure of spine remodeling in the MFC, yet there was no difference in mean spine density at P25, during the peak of adolescent spine remodeling (Fig 5D). This could potentially be due to complementary mechanisms in non-Nex1-expressing neurons and glia compensating for the loss of AnkB in pyramidal neurons early during adolescence, but by the end of the remodeling phase the loss of AnkB becomes apparent. An alternative explanation could be that the spine remodeling phase is not one homogenous mechanism, but a collection of distinct mechanisms which show a temporal regulation within the spine remodeling phase. Potentially the Sema3F-NrCAM spine remodeling and other AnkB-interacting signaling components occurs after P25, and as such no difference is seen with loss of AnkB prior to this timepoint. Further experiments need to be conducted to delineate the role of timing *in vivo*. Moreover, an *in vitro* neuron culture system would be

informative for exploring the direct role of AnkB in the Sema3F-NrCAM-Npn2-PlexA3 holoreceptor complex and downstream RapGAP signaling through PlexA3.

Elucidating the role that cytoskeletal components DCLK1 and AnkB play in Sema3F-mediated dendritic spine retraction during development may translate into knowledge about how the brain rewires itself on a subcellular mechanistic level. Characterization of the proteins in this complex, combined with genetic studies in human neurodevelopmental disorders could present a potential target for small molecular drug therapies or the more recent adeno-associated virus (AAV) and Crispr/Cas9 gene-editing systems.[35–37] As dendritic spines are the major site of excitatory signaling in the mammalian brain, it is important to increase our understanding of how this system is regulated for establishing healthy connectivity. Too many, as well as too few, dendritic spines can have profound effects on human cognition.[5] In addition to a decreased quality of life for the affected individual and family, it also creates a financial burden for society as a whole. Biochemical insights into this process can help to address the gaps in our knowledge of how and why these diseases develop, and contribute to our final goal of rescuing healthy functioning in affected individuals.

REFERENCES

Huttenlocher PR. (1979) Synaptic density in human frontal cortex - developmental changes and effects of aging. *Brain Res*. 163(2):195-205.

Holtmaat A, Svoboda K. (2009) Experience-dependent structural synaptic plasticity in the mammalian brain. *Nat Rev Neurosci*. 10(9):647-658.

McAllister AK. (2007) Dynamic Aspects of CNS Synapse Formation. *Annu Rev Neurosci*. 30(1):425-450.

Petanjek Z, Judaš M, Šimic G, Rasin MR, Uylings HBM, Rakic P, Kostovic I. (2011) Extraordinary neoteny of synaptic spines in the human prefrontal cortex. *Proc Natl Acad Sci U S A*. 108(32):13281-13286.

Penzes P, Cahill ME, Jones KA, Vanleeuwen JE, Woolfrey KM. (2011) Dendritic spine pathology in neuropsychiatric disorders. *Nat Neurosci*. 14(3):285-293.

Tran TS, Rubio ME, Clem RL, Johnson D, Case L, Tessier-Lavigne M, Huganir RL, Ginty DD, Kolodkin AL. (2009) Secreted Semaphorins Control Spine Distribution and Morphogenesis in the Postnatal CNS. *Nature*. 462(7276):1065.

Kolodkin AL, Tessier-Lavigne M. (2011) Mechanisms and Molecules of Neuronal Wiring: A Primer. *Cold Spring Harb Perspect Biol*. 3(6):a001727-a001727.

Demyanenko GP, Mohan V, Zhang X, Brennaman LH, Dharbal KES, Tran TS, Manis PB, Maness PF. (2014) Neural Cell Adhesion Molecule NrCAM Regulates Semaphorin 3F-Induced Dendritic Spine Remodeling. *J Neurosci*. 34(34):11274-11287.

Sheng M, Kim E. (2011) The Postsynaptic Organization of Synapses. *Cold Spring Harb Perspect Biol*. 3(12):1-21.

Dent EW. (2017) Of microtubules and memory: implications for microtubule dynamics in dendrites and spines. *Mol Biol Cell*. 28(1):1-8.

Yan Z, Kim E, Datta D, Lewis DA, Soderling SH. (2016) Synaptic Actin Dysregulation, a Convergent Mechanism of Mental Disorders? *J Neurosci*. 36(45):11411-11417.

Dai J, Dalal JS, Thakar S, Henkemeyer M, Lemmon VP, Harunaga JS, Schlatter MC, Buhusi M, Maness PF. (2012) EphB regulates L1 phosphorylation during retinocollicular mapping. *Mol Cell Neurosci*. 50(2):201-210.

Irimia M, Weatheritt RJ, Ellis JD, Parikshak NN, Gonatopoulos-Pournatzis T, Babor M, Quesnel-Vallières M, et al. (2014) A highly conserved program of neuronal microexons is misregulated in autistic brains. *Cell*. 159(7):1511-1523.

Iossifov I, Ronemus M, Levy D, Wang Z, Hakker I, et al. (2012) De Novo Gene Disruptions in Children on the Autistic Spectrum. *Neuron*. 74(2):285-299.

Willsey AJ, Sanders SJ, Li M, Dong S, Tebbenkamp AT, et al. (2013) Coexpression networks implicate human midfetal deep cortical projection neurons in the pathogenesis of autism. *Cell*. 155(5):997-1007.

De Rubeis S, He X, Goldberg AP, Poultney CS, Samocha K, et al. (2014) Synaptic, transcriptional and chromatin genes disrupted in autism. *Nature*. 515(7526):209-215.

Iossifov I, Levy D, Allen J, Ye K, Ronemus M, Lee Y-H, Yamrom B, Wigler M. (2015) Low load for disruptive mutations in autism genes and their biased transmission. *Proc Natl Acad Sci U S A*. 112(41):E5600-7.

Scotland P, Zhou D, Benveniste H, Bennett V. (1998) Nervous system defects of AnkyrinB (-/-) mice suggest functional overlap between the cell adhesion molecule L1 and 440-kD AnkyrinB in premyelinated axons. *J Cell Biol*. 143(5):1305-1315.

Kizhatil K, Wu Y-X, Sen A, Bennett V. (2002) A new activity of doublecortin in recognition of the phospho-FIGQY tyrosine in the cytoplasmic domain of neurofascin. *J Neurosci*. 22(18):7948-7958.

Yap CC, Vakulenko M, Kruczek K, Motamedi B, Digilio L, Liu JS, Winckler B. (2012) Doublecortin (DCX) Mediates Endocytosis of Neurofascin Independently of Microtubule Binding. *J Neurosci*. 32(22):7439-7453.

Yap CC, Winckler B. (2015) Adapting for endocytosis: roles for endocytic sorting adaptors in directing neural development. *Front Cell Neurosci*. 9:119.

Shin E, Kashiwagi Y, Kuriu T, Iwasaki H, Tanaka T, Koizumi H, Gleeson JG, Okabe S. (2013) Doublecortin-like kinase enhances dendritic remodelling and negatively regulates synapse maturation. *Nat Commun*. 4:1414-1440.

Chung W-S, Clarke LE, Wang GX, Stafford BK, Sher A, Chakraborty C, Joung J, Foo LC, Thompson A, Chen C, Smith SJ, Barres BA. (2013) Astrocytes mediate synapse elimination through MEGF10 and MERTK pathways. *Nature*. 504(7480):394-400.

Wu Y, Dissing-Olesen L, MacVicar BA, Stevens B. (2015) Microglia: Dynamic Mediators of Synapse Development and Plasticity. *Trends Immunol*. 36(10):605-613.

Tremblay M-È, Majewska AK. (2011) A role for microglia in synaptic plasticity? *Commun Integr Biol*. 4(2):220-222.

Di Polo A. (2015) Dendrite pathology and neurodegeneration: focus on mTOR. *Neural Regen Res*. 10(4):559-561.

Henry FE, Hockeimer W, Chen A, Mysore SP, Sutton MA. (2017) Mechanistic target of rapamycin is necessary for changes in dendritic spine morphology associated with long-term potentiation. *Mol Brain*. 10(1):50

Smith SA, Sturm AC, Curran J, Kline CF, Little SC, Bonilla IM, et al (2015) Dysfunction in the βII Spectrin–Dependent Cytoskeleton Underlies Human Arrhythmia. *Circulation*. 131(8):695-708.

Agarwal A, Dibaj P, Kassmann CM, Goebbels S, Nave K-A, Schwab MH. (2012) In vivo imaging and noninvasive ablation of pyramidal neurons in adult NEX-CreERT2 mice. *Cereb Cortex*. 22(7):1473-1486.

Villasana LE, Klann E, Tejada-Simon MV. (2006) Rapid isolation of synaptoneurosomes and

postsynaptic densities from adult mouse hippocampus. *J Neurosci Methods*. 158(1):30-36.

Mohan V, Sullivan CS, Guo J, Wade SD, Majumder S, Agarwal A, Anton ES, Temple BS, Maness PF. (2018) Temporal Regulation of Dendritic Spines Through NrCAM-Semaphorin3F Receptor Signaling in Developing Cortical Pyramidal Neurons. *Cereb Cortex*. (February):1-15.

Demyanenko GP, Tsai AY, Maness PF. (1999) Abnormalities in neuronal process extension, hippocampal development, and the ventricular system of L1 knockout mice. *J Neurosci*. 19(12):4907-4920.

Buhusi M, Schlatter MC, Demyanenko GP, Thresher R, Maness PF. (2008) L1 Interaction with Ankyrin Regulates Mediolateral Topography in the Retinocollicular Projection. *J Neurosci*. 28(1):177-188.

Brabander M De, Geuens G, Nuydens R, Willebrords R, Aerts F, Mey J De, Mcintosh JR. (1986) Microtubule Dynamics during the Cell Cycle: The Effects of Taxol and Nocodazole on the Microtubule System of Pt K2 Cells at Different Stages of the Mitotic Cycle. *Int Rev Cytol*. 101:215-274.

Soriano V. (2017) Hot News: Gene Therapy with CRISPR/Cas9 Coming to Age for HIV Cure. *AIDS Rev*. 19(3):167-172.

Mollanoori H, Teimourian S. Therapeutic applications of CRISPR/Cas9 system in gene therapy. (2018) *Biotechnol Lett*. 40(6):907-914.

Naso MF, Tomkowicz B, Perry WL, Strohl WR, Strohl WR. (2017) Adeno-Associated Virus (AAV) as a Vector for Gene Therapy. *BioDrugs*. 31(4):317-334.

CHAPTER TWO: TEMPORAL REGULATION OF DENDRITIC SPINES THROUGH NrCAM-SEMAPHORIN-3F RECEPTOR SIGNALING IN DEVELOPING CORTICAL PYRAMIDAL NEURONS[1]

INTRODUCTION

Neurocan is a chondroitin sulfate proteoglycan present in perineuronal nets, which are associated with closure of the critical period of synaptic plasticity. During postnatal development of the neocortex dendritic spines on pyramidal neurons are initially overproduced; later they are pruned to achieve an appropriate balance of excitatory to inhibitory synapses. Little is understood about how spine pruning is terminated upon maturation. NrCAM (Neuron-glial related cell adhesion molecule) was found to mediate spine pruning as a subunit of the receptor complex for the repellent ligand Semaphorin 3F (Sema3F). As shown here in the postnatal mouse frontal and visual neocortex, Neurocan was localized at both light and electron microscopic level to the cell surface of cortical pyramidal neurons and was adjacent to neuronal processes and dendritic spines. Sema3F-induced spine elimination was inhibited by Neurocan in cortical neuron cultures. Neurocan also blocked Sema3F-induced morphological retraction in COS-7 cells, which was mediated through NrCAM and other subunits of the Sema3F holoreceptor, Neuropilin-2, and PlexinA3. Cell binding and ELISA assays demonstrated an association of Neurocan with NrCAM. Glycosaminoglycan chain interactions of Neurocan were required for inhibition of Sema3F-induced spine elimination, but the C-terminal sushi domain

[1] This chapter previously appeared as an article in the journal Frontiers in Cellular Neuroscience. The author contributed to immunofluorescence staining and co-immunoprecipitation pull down experiments. The original citation is as follows: Mohan V, Wyatt EV, Gotthard I, Phend KD, Duncan BW, Weinberg RJ, Tripathy A, Maness PF. (2018) Neurocan inhibits Semaphorin3F induced dendritic spine remodeling through NrCAM in cortical neurons. *Frontiers in Cellular Neuroscience*. 12:346.

was dispensable. These results describe a novel mechanism wherein Neurocan inhibits NrCAM/Sema3F-induced spine elimination.

MATERIALS AND METHODS

Mice

Wild type (WT) and NrCAM null mutant mice in the C57BL/6 genetic background were maintained in a 12-h day and night cycle environment with *ad libitum* availability of chow diet and water. For labeling postmitotic pyramidal neurons in the cerebral cortex, Nex1-CreERT2 mice were crossed with the RCE reporter strain (both in C57Bl/6) to generate a tamoxifen-inducible reporter line of mice expressing EGFP in postmitotic pyramidal neurons under the control of Nex1-Cre as previously characterized.[1,2] Recombination-induced expression of EGFP in postmitotic pyramidal neurons was achieved by daily injections of tamoxifen (100mg/kg in sunflower oil) from postnatal day P10-13, as described.[1,2] Mice were sacrificed at post-induction timepoints using approved methods. All animal experiments were approved by the Institutional Animal Care and Use Committee of The University of North Carolina School of Medicine at Chapel Hill (IACUC Protocol # 15-114). Mice were handled according to the University of North Carolina Institutional Animal Care and Use Committee policies and in accordance with NIH guidelines for humane care and use of laboratory animals.

Immunoblotting

Lysates of mouse cortex (P7, P14, P21, and P80) and cell cultures were prepared in lysis buffer (1% Brij98, 10 mM Tris-Cl pH 7.0, 150 mM NaCl, 1 mM NaEDTA, 1 mM NaEGTA, 200 μM Na3VO4, 10 mM NaF, and 1X protease inhibitors (Sigma-Aldrich). Lysates (50 μg) were subjected to Western blotting with the following antibodies: anti-NrCAM (1:1000, Abcam), anti-Neurocan (1:500, R&D), anti-Sema3F (1:500, Millipore), and anti-β actin (1:1000, Millipore). Blots were developed with HRP-tagged secondary antibodies (1:5000, Jackson Immunoresearch) using Western Bright ECL Substrate (Advansta) and light sensitive radiometric film exposure. Bands were quantified by densitometry using BioRad ImageLab software.

Immunostaining

For immunostaining, neuronal cultures transfected with pCAGGS-IRES-mEGFP were fixed at DIV14 in 4% paraformaldehyde (PFA), permeabilized with Triton X-100, blocked in 10% horse or donkey serum, and labeled with chicken anti-GFP (Abcam). Secondary anti-chicken Alexa Fluor 488 antibodies (1:500) were added for 1 h before mounting and confocal imaging. For Neurocan localization, 100 μm coronal brain sections were prepared on vibratome from Nex1-CreERT2:Ai9 mice (P18 and P80) expressing tdTomato in pyramidal neurons. Serial 100 μm vibratome sections from P18 and P80 brain were matched for level based on rostrocaudal distance from the anterior end of the brain. Samples were blocked in PBS, 10% donkey serum, 0.3% Triton X100, then incubated with Neurocan antibodies (1:500, R&D) for 24 h at 4°C, then with anti-sheep Alexa Fluor 488 secondary antibody (1:500). After washing, sections were mounted with Prolong Gold anti-fade reagent (Invitrogen) and imaged using a Zeiss LSM 700 confocal microscope. All images were captured using identical microscope settings, we kept the total z thickness (7.35 μm) as well as thickness of single optical sections (0.35 μm) same for all samples. tdTomato (red) fluorescence was excluded from analysis. The intensity of total Neurocan fluorescence observed in the green channel was quantified for each image after auto-thresholding without regard to tdTomato fluorescence. Quantification of pixel intensity was performed blindly using ImageJ software (NIH).

Neurocan immunogold labeling and electron microscopy

C57BL/6 WT mice (P18 and P80) were anesthetized and perfused transcardially with phosphate buffer (0.15 M sodium phosphate, pH 7.4) and postfixed in 4% PFA, 0.1% glutaraldehyde in PBS. Coronal vibratome sections (50 μm) were subjected to pre-embedding immunogold labeling with silver enhancement using Neurocan antibodies and streptavidin-

nanogold (Nanoprobes 2016), as we previously described.[3] Sections were silver-enhanced using HQ silver enhancement kit (Nanoprobes 2012), and post-fixed in osmium tetroxide. Sections were then stained with uranyl acetate and infiltrated with resin. Tissue was sectioned (50–60 nm), collected on 300 mesh nickel or copper grids, counterstained with uranyl acetate and Sato's lead and examined with a Tecnai 12 transmission electron microscope.

Spine retraction assay in cortical neuron cultures

Cortical neuronal cultures were prepared from mouse embryos (E15.5) and plated on laminin, poly-D-lysine coated chamber slides. Neurons were maintained in neurobasal medium (Gibco) supplemented with B27 and antibiotics. Cells were transfected with plasmid pCAGGS-IRES-mEGFP at DIV11 using Lipofectamine 2000 (Thermo Fisher Scientific). Transfected cells at DIV14 were treated with 3 nM Sema3F-Fc (R&D) or Fc (Abcam) for 30 min, the time at which spines are maximally retracted.[2] Where indicated, cultures were pre-treated for 30 min with 8–20 nM full length recombinant human Neurocan (Glu23-Cys1321, R&D) or a mouse Neurocan fragment (Asp23-Asp637, R&D), which lacks the C-terminal sushi domain and approximately half of the GAG-modified region. Cells were fixed in 4% PFA, permeabilized with Triton X-100, blocked in 10% serum, and labeled with anti-GFP to enhance visualization of spines. Spine densities were scored on the first branch of multiple apical dendrites using Neurolucida software. Spine analysis was blinded. Data was collected from confocal images of EGFP-labeled neurons with pyramidal morphology in each of four replicate cultures. Mean spine densities ± SEM were compared by the *t*-test (2-tailed, unequal variances, $p < 0.05$). To test the effect of GAG chain digestion, Neurocan was incubated in solution with 0.1 units/μg chondroitinase ABC (chABC, Sigma) at 37°C for 1.5 h, followed by heat inactivation of enzyme at 100°C for 10 min. Efficacy of GAG digestion was assessed by immunoblotting.

COS-7 cell retraction assay

COS-7 cells were plated on eight well chamber slides (25,000 cells/well) coated with poly-D-lysine. The following day cells were transfected with plasmids expressing NrCAM (pCMV6), Npn2 (pCOS), and/or PlexA3-EGFP (pCAGGS-PlexA3-IRES-mEGFP). At 48 h after transfection cells were treated with 3 nM Sema3F-Fc or Fc for 30 min, subjected to immunofluorescence staining for GFP and imaged on confocal microscope. The particle tool of ImageJ was used after auto-thresholding to measure the area of individual labeled cells. The software auto-detects the boundary of cells in thresholded images. Cells between 500 and 1000 μm^2 were classified as retracted (collapsed), and those greater than 1000 μm^2 were classified as non-retracted. The mean percent of collapsed cells relative to the total GFP-positive cells was calculated from three experiments, 10 images per condition, and compared by the *t*-test for significant differences ($^{*}p < 0.05$, $n = 3$ from ~200 cells/image). Preliminary dose response experiments showed that Neurocan (4–40 nM) effectively inhibited the Sema3F-Fc-induced COS-7 cell retraction response; we selected 8 nM for subsequent studies.

Cell binding and ELISA assays

COS-7 cells were transfected with NrCAM in pCMV6 or vector alone, together with pCAGGS-IRES-mEGFP. Cortical neurons from NrCAM homozygous null mice were transfected on DIV11 with pCAGGS-NrCAM-IRES-mEGFP or vector alone. At 48 h post-transfection, cells were treated with 20 nM recombinant Neurocan at 37°C for 30 min. To assay Neurocan binding to the cell surface, cultures were fixed and subjected to indirect immunofluorescence staining with antibodies to Neurocan and secondary Alexa Fluor-conjugated antibodies. Single optical section images were taken on the confocal microscope

using the same settings for each condition, and the fluorescence intensity of staining measured using Image J.

ELISA was performed to measure the binding between NrCAM-Fc (R&D) and alkaline-phosphatase-tagged Neurocan (Neurocan-AP). The Neurocan-AP fusion protein construct was generated by PCR amplification of full-length mouse Neurocan cDNA (Accession: BC065118), followed by subcloning into the APtag5 vector so that the alkaline phosphatase (AP) tag was inserted at the N-terminus of Neurocan.[4] Neurocan-AP or AP control proteins were harvested from conditioned media of HEK293T cells transfected with Neurocan-APtag5 or APtag5 plasmids after 72 h. Media was clarified by centrifugation and filtered through a 0.45 μm filter. Detailed methods of APtag5 protein production have been described.[5] The ELISA was carried out essentially as described for Neurocan-AP binding to protein tyrosine phosphatase sigma.[4] Protein A plates (Pierce) were coated with 1 μM NrCAM-Fc or Fc in HBSS-20 mM HEPES, pH 7.0 for 2 h at room temperature. Blocking was performed with SuperBlock (Thermo Fisher Scientific). After washing in HBSS-20 mM HEPES, wells were incubated with 10 μM Neurocan-AP or AP for 1.5 h at RT. Reaction product was developed using p-nitrophenylphosphate to detect AP activity. Optical density measurements were taken at 405 nm on an ELISA plate reader.

To assess direct binding of Neurocan with semaphorins, 1 μg of full length recombinant Neurocan (R&D) was incubated with 1 μg of either control Fc, Sema3A-Fc, or Sema3F-Fc in Tris-buffered saline for 1 h at 37°C. Protein A/G Sepharose beads were used to pull down Fc proteins for detection of bound Neurocan by immunoblotting with Neurocan antibodies. Blots were reprobed with anti-Fc antibodies.

RESULTS

Expression and localization of Neurocan in the frontal and visual cortex

To evaluate the postnatal expression of Neurocan in developing mouse brain, cortical lysates were analyzed at P7, P14, P30, and adult by Western blotting. Neurocan was detected as a broad band from 150 to 250 kDa reflecting GAG-modification (Fig. 6A). Quantification showed that Neurocan expression in the cortex increased markedly (~8 fold) from P7 to P14, declined at P30, and persisted in adulthood (Fig. 6A,B). The level of Sema3F (90 kDa) in the developing cortex paralleled that of Neurocan with a ~6 fold increase from P7 to P14 then a decrease with maturation (Fig. 6A,B). To determine if Neurocan was localized to cortical pyramidal neurons at adolescent (P18) and adult (P80) stages, immunofluorescence staining for Neurocan was performed in the medial frontal cortex (MFC) and primary visual cortex (V1). These cortical regions have been shown to be sites of spine density regulation on apical dendrites of pyramidal neurons by Sema3F and NrCAM/Npn2/PlexA3.[2] To identify pyramidal neurons, we used a tamoxifen-inducible reporter line of mice expressing tdTomato specifically in postmitotic pyramidal neurons under the control of Nex1-CreERT2 promoter.[1,2] At both P18 and P80, Neurocan labeling in the MFC and V1 was prominent around cell bodies and processes of tdTomato-positive pyramidal neurons throughout the cortical layers, in addition to other cells (Fig. 6C). Nonimmune IgG (IgG) staining was negligible. The intensity of Neurocan immunofluorescence (green channel only, excluding tdTomato) was quantified in coronal sections matched for level from confocal images obtained under identical settings. Neurocan immunofluorescence levels throughout the cortical layers were significantly greater at P18 than P80 in both the MFC and V1 (Fig. 6D). At higher magnification Neurocan labeling

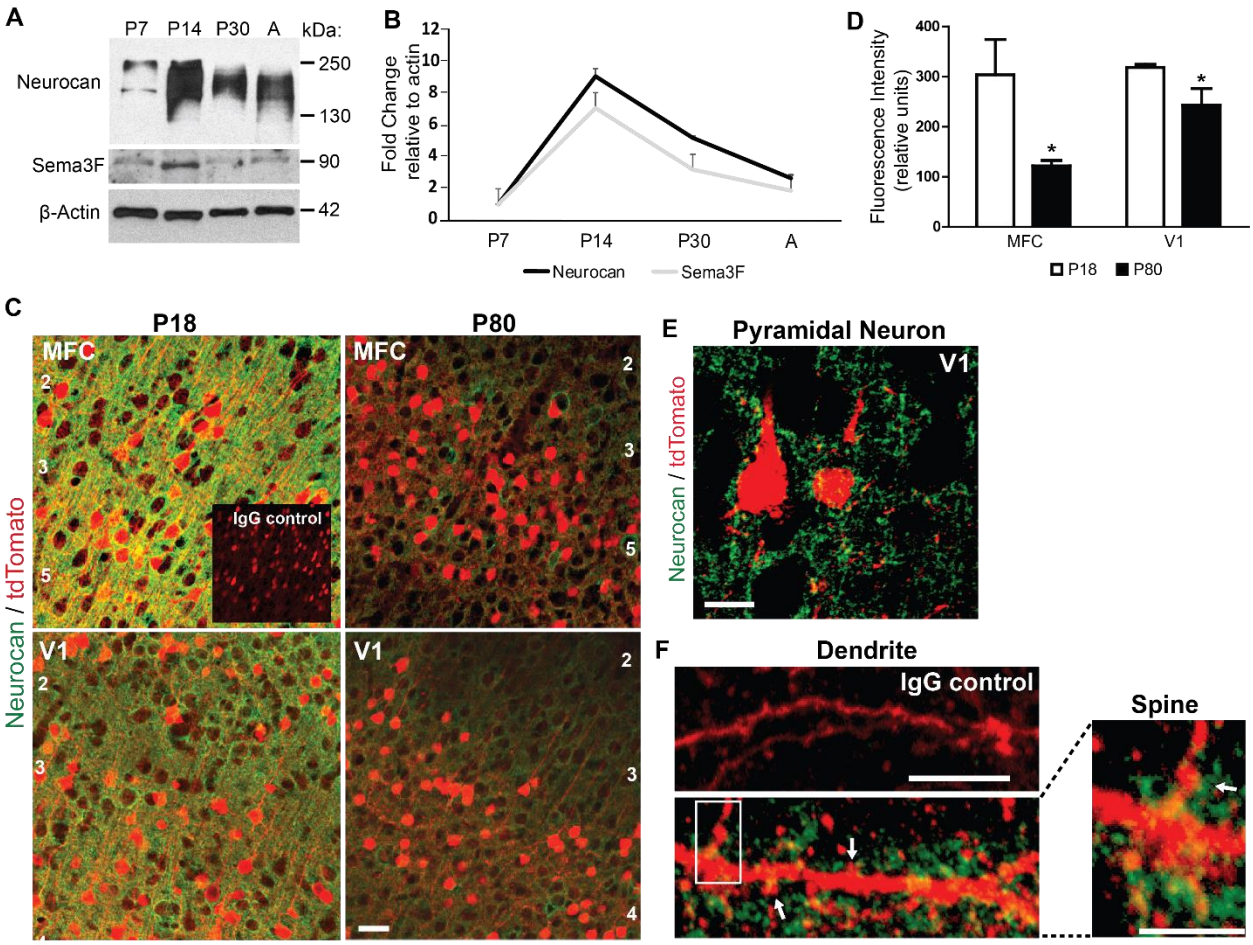

Figure 6: Expression of Neurocan in developing mouse neocortex. (A) Representative immunoblots of Neurocan and Sema3F in lysates of cerebral cortex (50 µg) from postnatal (P7, P14, P30) and adult brain (A). β-Actin served as loading control. (B) Relative levels of Neurocan and Sema3F in cerebral cortex (A) at each developmental stage (n=3) normalized to β-actin. Means ± SEM are shown. (C) Immunofluorescence staining for Neurocan (green) and tdTomato (red) in coronal sections from MFC and V1, layer 4 in Nex1-CreERT2:Ai9 mice at adolescent (P18) and adult (P80) stages. Nonimmune IgG control is shown as an inset. Cortical layers are numbered. Scale bar = 50µm. (D) Fluorescence intensity of Neurocan immunostaining in MFC and V1 at P18 and P80 (n=10 images for each condition from 3 brains). Mean differences (± SEM) in Fc versus Sema3F-Fc treated cultures were compared for significance (*t-test, $p<0.05$). (E) Representative image showing Neurocan immunostaining (green) surrounding tdTomato-positive pyramidal neurons in V1, of Nex1-CreERT2:Ai9 mice. Scale bar = 50 µm. (F) High magnification of E. Upper panel, normal IgG; lower panel, Neurocan immunostaining (green) around dendrites with spines (scale bar = 10µm). Far right panel shows magnified view of boxed area.

of pyramidal neurons at P18 in the MFC appeared to be diffusely localized around soma, dendrites, and extracellular space (Fig. 6E). Neurocan was also evident as a diffuse net at or near the membrane of dendritic branches, including in the vicinity of dendritic spines (arrows, Fig. 6F).

The subcellular localization of Neurocan was investigated in greater detail in the MFC by

immunogold labeling at the electron microscope level. At P18, labeled Neurocan was observed near the neuronal membrane adjacent to excitatory, asymmetric synapses of dendritic spines (Sp; Fig. 7A, arrows) but it was not found directly within synaptic junctions. Neurocan was also evident at the membrane or extracellular space, and could be seen near presynaptic axon terminals (AT), which harbored synaptic vesicles (Fig. 7A,B,D, arrows). Neurocan labeling was frequently clustered at or near dendritic membranes as well as the extracellular space (Fig. 7C, arrows). At P80, Neurocan was observed at the plasma membrane near spines, and sometimes adjacent to asymmetric, excitatory synapses (Fig. 7E). At both stages labeling was rarely present within the cytoplasm. The appropriate dilution of Neurocan antibodies and specificity was pre-assessed by immunoperoxidase staining of COS-7 cells transfected with plasmids expressing Neurocan-AP or control AP protein. Cells expressing Neurocan-AP were clearly stained with Neurocan antibodies, whereas cells expressing AP elicited minimal staining, as did omission of primary antibody (Fig. 7F). In summary, Neurocan was expressed prominently in the postnatal MFC and V1, declining with maturation, and was localized near the plasma membrane of pyramidal cell processes and adjacent to dendritic spines.

Neurocan inhibits Sema3F-induced spine and cell retraction

To assess the potential of Neurocan to terminate spine remodeling during postnatal maturation, we tested the ability of Neurocan to inhibit Sema3F-induced spine retraction in cortical neurons in culture. In this assay,[2,6] dissociated cortical neurons from mouse embryos at E15.5 were transfected with pCAGGS-IRES-mEGFP at DIV11 and cultured to DIV14. Cells were pre-treated with or without Neurocan for 30 min, then stimulated with 3 nM Sema3F-Fc or Fc protein for 30 min. We used a concentration of Neurocan (20 nM) that exceeded the Kd for Neurocan binding to L1-CAM (~1 nM)[7,8] effectively inhibited ephrinA5-induced axon terminal

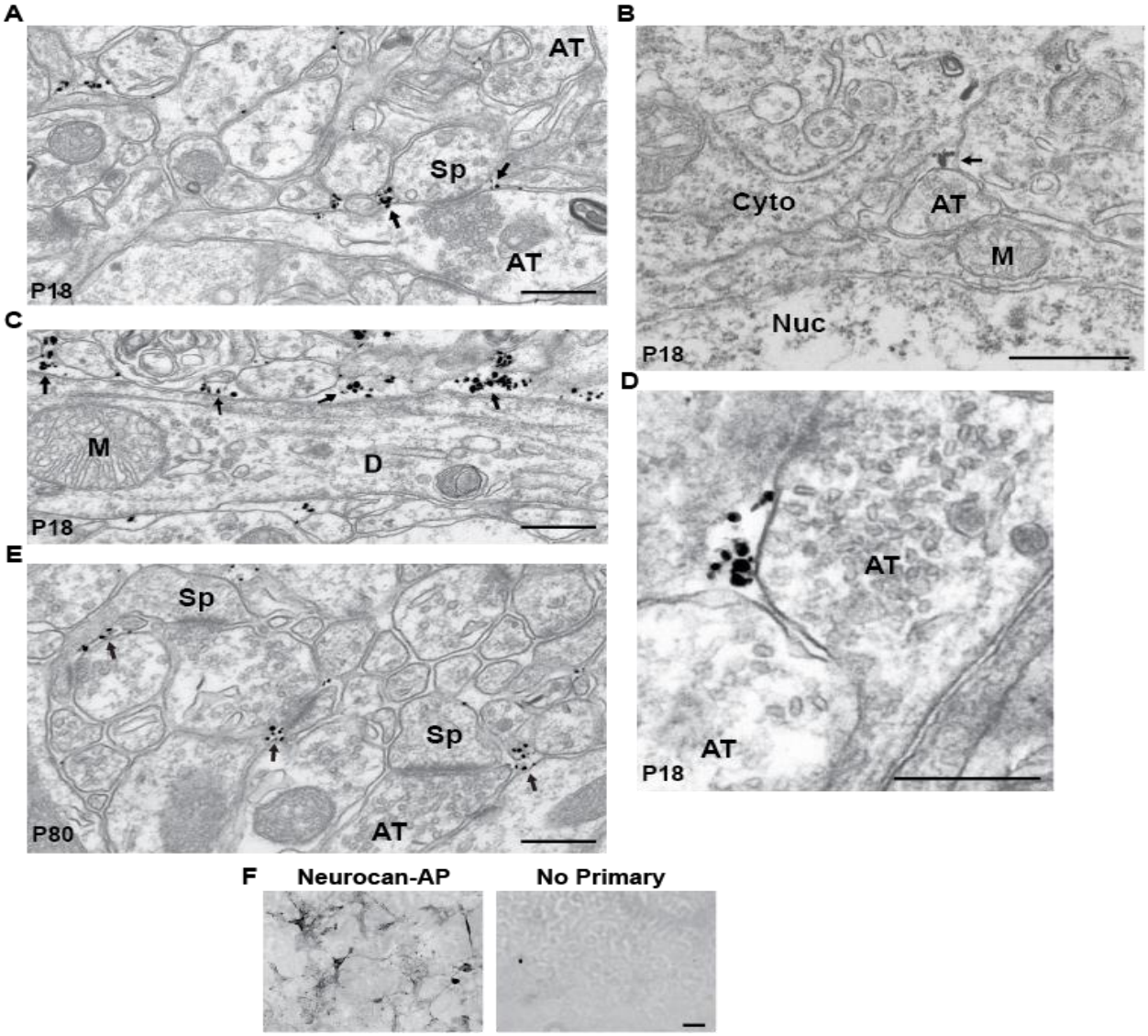

Figure 7: Localization of Neurocan in mouse medial frontal cortex (MFC) by immunogold labeling and electron microscopy. (A) Electron micrograph of MFC layer 2/3 at P18, showing immunogold labeling of Neurocan near the plasma membrane adjacent to a spine (Sp) and axon terminal (AT) (arrows). (B) Neurocan labeling in the extracellular space near an axon terminal (AT; arrow) at P18. Nucleus (Nuc), cytoplasm (Cyto). (C) Accumulation of Neurocan (arrows) in extracellular space and along the plasma membrane of a dendrite (D) at P18. Mitochondria (M) were unlabeled. (D) Neurocan labeling adjacent to axon terminals (AT) at P18. (E) Neurocan labeling at neck of spine (Sp) and near excitatory synapses (arrows) at P80. Scale bar = 1μm. (F) Validation of Neurocan antibody specificity by immunoperoxidase staining of COS-7 cells transfected with Neurocan-AP or AP alone in the APtag5 vector, using Neurocan antibodies or no primary antibody. An antibody dilution series was carried out in pilot experiments. Scale bar = 50 μm.

retraction in cortical neuron cultures,[3] and was within the estimated physiological range in rodent brain, which varies with age and region.[9,10] Analysis of spine density on apical dendrites of EGFP-labeled neurons showed that Neurocan (20 nM) blocked Sema3F-induced spine retraction, but had no effect on spine density of Fc-treated neurons (Fig. 8A,B). Similar results in neuronal

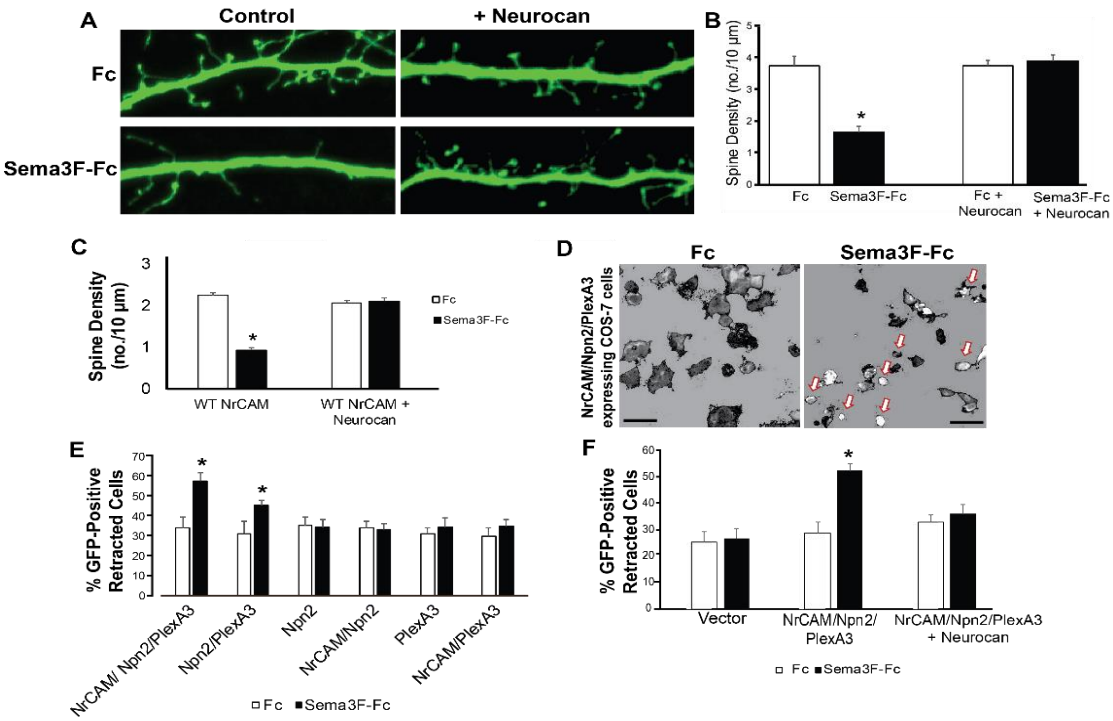

Figure 8: Neurocan inhibits Sema3F-induced spine and cell retraction. (A) Apical dendrites and spines of mouse cortical neurons expressing EGFP in cultures treated with Fc or Sema3F-Fc for 30 min. Pretreatment with 20 nM Neurocan for 30 min prevented Sema3F-Fc induced spine collapse but did not affect spine density in Fc-treated control cultures. Scale bar = 10µm. (B) Quantification of experiment in panel A, showing significant reduction in mean spine density upon Sema3F-Fc treatment by Neurocan (n=3, 10 neurons per condition; *p<0.05, t- test). (C) Treatment with 8 nM Neurocan for 30 min also prevented Sema3F-Fc induced spine collapse and did not affect spine density in Fc-treated control cultures (n=3, 10 neurons per condition; *p<0.05, t- test). (D) Representative thresholded images showing morphological retraction of COS-7 cells expressing NrCAM, Npn2, PlexA3 and EGFP after Sema3F-Fc treatment compared to Fc. Arrows point to retracted cells. Scale bar = 100µm. (E) Quantification of morphological cell retraction after Fc or Sema3F-Fc treatment of COS-7 cells expressing NrCAM, Npn2, and/or PlexA3 and EGFP in panel A. Results show percent retracted cells (n=3 assays, *p<0.05, t test). (F) Quantification of morphological retraction upon Fc or Sema3F-Fc treatment of COS-7 cells expressing NrCAM, Npn2, and PlexA3 with and without pre-treatment with 20 nM Neurocan for 30 min (n=3 assays, *p<0.05, t test).

cultures with a lower spine density were obtained using a lower concentration of Neurocan (8 nM) **(**Fig. 8C).

To evaluate the molecules involved, we used a heterologous assay in which morphological retraction of COS-7 cells can be induced by Sema3A-Fc or Sema4D-Fc.[11] COS-7 cells were transfected with one or more plasmids expressing NrCAM, Npn2, PlexA3, then treated with 3 nM Sema3F-Fc or Fc for 30 min. COS-7 cells expressing all three Sema3F holoreceptor subunits NrCAM, Npn2, and PlexA3, showed the highest percent of retracted cells

after treatment with Sema3F-Fc compared to Fc (Fig. 8D,E**)**. Cells expressing only Npn2 and PlexA3 also retracted upon Sema3F-Fc treatment but required NrCAM for maximal response (Fig. 8E). Significant retraction was not observed in COS-7 cells expressing Npn2 or PlexA3 alone, or in cells doubly expressing NrCAM/Npn2 or NrCAM/PlexA3 (Fig. 8E). Cells expressing only EGFP also did not respond to Sema3F-Fc (Fig. 8F). A basal level of retracted cells was observed in each condition (25–30%), which may be due to changes in shape as a result of mitosis, migration, or cell heterogeneity. To determine if Neurocan negatively regulated Sema3F-induced cell retraction, COS-7 cells expressing NrCAM/Npn2/PlexA3 were pre-treated with 8 nM Neurocan, then stimulated with 3 nM Sema3F-Fc or Fc. Neurocan effectively blocked NrCAM/Npn2/PlexA3-dependent retraction to Sema3F-Fc (Fig. 8F). These results demonstrated that Neurocan negatively regulates Sema3F-induced retraction through a mechanism involving the NrCAM/Npn2/PlexA3 receptor complex.

NrCAM-dependent binding of Neurocan

We hypothesized that Neurocan negatively regulates Sema3F-mediated retraction by binding to the extracellular region of NrCAM at the cell surface. To test this, we examined the ability of Neurocan to bind to COS-7 cells transfected with NrCAM or vector alone, together with EGFP. COS-7 cells were treated 48 h post-transfection with or without 20 nM Neurocan for 30 min. Cells were washed extensively, fixed without permeabilization, and subjected to immunofluorescence staining with Neurocan antibodies. The amount of surface-bound Neurocan on EGFP-labeled cells was quantified by measuring the fluorescence intensity of Neurocan staining in single optical sections. Results showed that Neurocan bound at greater levels to the surface of cells that expressed NrCAM compared to cells without NrCAM transfected with vector alone (Fig. 9A,B). The low level of fluorescence seen in untreated cells was likely nonspecific. Immunoblotting for Neurocan and GAPDH (loading control) in lysates of similarly

treated cells, showed that Neurocan was detected in cells transfected with the NrCAM plasmid but not in control cells without NrCAM (Fig. 9C).

To determine if Neurocan bound to neuronal cells expressing NrCAM, cortical neuron cultures from homozygous NrCAM null mutant embryos (E15.5) were transfected at DIV11 with pCAGGS-IRES-mEGFP or pCAGGS-NrCAM-IRES-mEGFP, and treated at DIV14 with 20 nM Neurocan for 30 min. After washing and fixation without permeabilization, neurons were immunostained to detect Neurocan on the cell surface. EGFP-labeled neurons expressing NrCAM exhibited a greater amount of surface-bound Neurocan than NrCAM-minus neurons, and quantitation showed that this difference was significant (Fig. 9D,E). The lower level of Neurocan fluorescence on NrCAM-minus neurons may be due to interaction with other binding proteins on the cell surface. Results of the cell binding assays showed that expression of NrCAM leads to increased binding of Neurocan to the cell surface. To assess a direct interaction of Neurocan with the NrCAM extracellular region, we developed an ELISA using purified, full-length mouse Neurocan fused to AP expressed in HEK293T cells. NrCAM-Fc protein was adsorbed to ELISA plates that were pre-coated with Protein A, then incubated with Neurocan-AP or AP control protein for 1.5 h. Binding was quantified by colorimetric detection of bound AP using p-nitrophenylphosphate. As a positive control, Neurocan-AP was also assayed for binding to NCAM, a different cell adhesion molecule known to engage Neurocan at its extracellular Ig2 domain.[3] Neurocan-AP bound to NrCAM-Fc to a significantly greater extent than control AP (Fig. 9F). Similar levels of Neurocan-AP binding to NCAM-Fc were observed. Taken together, these results support the conclusion that Neurocan binds to the extracellular region of NrCAM and inhibits Sema3F- mediated spine elimination in maturing pyramidal neurons of the mouse neocortex.

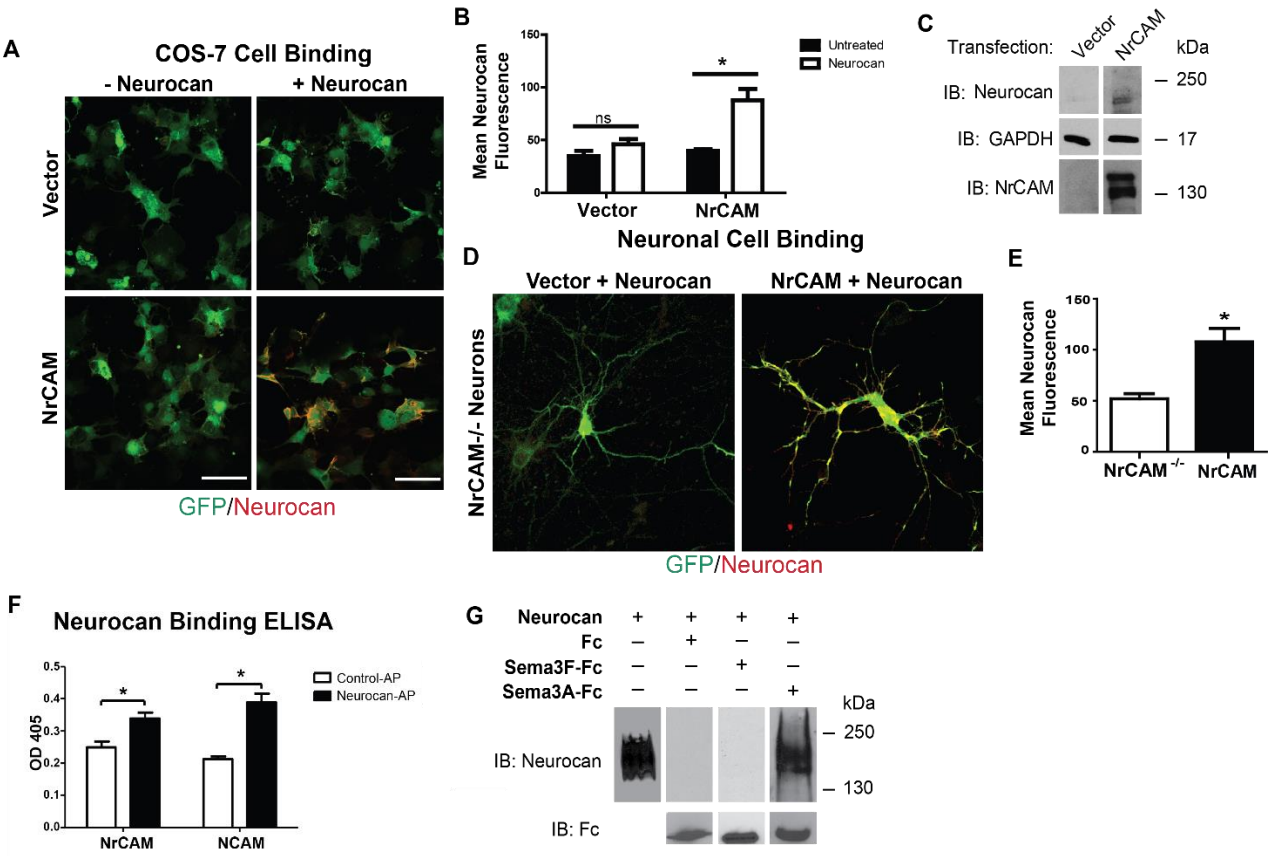

Figure 9: Cell binding and Neurocan interaction with NrCAM. (A) COS-7 cells transfected with vector alone (pCAGGS-IRES-mEGFP) or pCAGGS-NrCAM-IRES-mEGFP were pre-treated with 8 nM Neurocan, then fixed and subjected to immunofluorescence staining without permeabilization to detect surface-bound Neurocan (red). Scale bar= 100 µm. (B) Mean fluorescence intensity (± SEM) of Neurocan immunofluorescence staining on the surface of COS-7 cells, as shown in panel A. NrCAM-expressing cells treated with Neurocan showed significantly greater levels of bound Neurocan than untreated cells. Fluorescence intensity in cells with vector alone treated with Fc or Sema3F-Fc was non-significant (ns). (*p>0.05, t test, n= 5 images each condition). (C) Lysates (50 µg) of cells transfected with vector alone or pCAGGS-NrCAM-IRES-mEGFP were treated with Neurocan as in panel A, and immunoblotted (IB) with Neurocan antibodies. Blots were reprobed with antibodies directed against GAPDH (loading control) or NrCAM (expression control). Representative immunoblots of 3 experiments are shown. (D) Mouse cortical neuron cultures from NrCAM null mice were transfected with vector alone or pCAGGS-NrCAM-IRES-EGFP, and pre-treated with 20 nM Neurocan before fixation and immunostaining to detect surface-bound Neurocan. In merged images of EGFP (green) and Neurocan (red), more Neurocan immunofluorescence was observed on the surface of neurons expressing NrCAM than on NrCAM null neurons with vector alone. (Scale bar= 50 µm). (E) Mean fluorescence intensity (± SEM) of surface-bound Neurocan immunostaining on neurons in panel D. NrCAM-expressing cells treated with Neurocan showed significantly greater levels of bound Neurocan than NrCAM-minus neurons. (*p>0.05, t-test, n= 10 neurons per condition). (F) ELISA of Neurocan-AP or control AP protein binding to NrCAM-Fc or positive control NCAM-Fc on protein A-coated microtiter wells. AP binding was detected colorimetrically with p-nitrophenylphosphate. The mean (± SEM) optical densities (OD 405) of Neurocan-AP bound to NrCAM-Fc or NCAM-Fc were significantly greater than control AP (t-test, *p>0.05). (G) Recombinant human Neurocan was incubated in Tris buffered saline with purified Fc, Sema3F-Fc, or Sema3A-Fc proteins, then complexes were pulled down with Protein A/G Sepharose beads. Immunoblotting for Neurocan showed no binding of Neurocan to Fc or Sema3F-Fc, whereas Neurocan bound effectively to Sema3A-Fc. Blots were reprobed with anti-Fc antibodies to demonstrate that equivalent amounts of Fc fusion proteins were pulled down. Recombinant Neurocan (left lane) ran as a broad band between 250 and 130 kDa.

Sema3A is a class 3 semaphorin that has been reported to bind to chondroitin sulfates in PNNs but has not been shown to bind Neurocan.[12,13] The possibility of sequestration of Sema3F-Fc by Neurocan was tested by incubating Sema3F-Fc, Sema3A-Fc, or Fc proteins in Tris buffered saline (TBS) with purified recombinant mouse Neurocan *in vitro*. Fc-containing protein complexes were pulled down with Protein A/G-Sepharose and subjected to Western blotting to detect Neurocan present in the Protein A/G pull-downs. Results showed that Neurocan bound to Sema3A-Fc, but there was no detectable association with Sema3F-Fc or Fc alone (Fig. 9G). Reprobing blots with anti-Fc antibodies confirmed that pull-downs contained approximately equivalent amounts of Fc-containing protein.

Importance of Neurocan GAG chains in regulation of spine retraction

CSPGs have been shown to restrict plasticity of cortical and hippocampal neurons, and digestion of their associated GAG chains with chondroitinase ABC (chABC) increases spine dynamics and density.[14-16] Therefore, we postulated that Neurocan GAG chains may be critical for inhibiting Sema3F-induced spine retraction. To test this hypothesis, GAG chains present on recombinant Neurocan were digested with chABC, as described.[3] Chondroitinase-digested Neurocan was compared with untreated Neurocan for inhibition of Sema3F-Fc induced spine retraction in cortical neuron cultures. Results showed that chABC-treated Neurocan (20 nM, 30 min) did not block Sema3F-induced spine retraction, whereas untreated Neurocan effectively inhibited spine retraction compared to the untreated control (Fig. 10A,B). GAG removal from Neurocan was confirmed on Western blots by a shift in GAG-modified Neurocan to lower molecular weight and band narrowing (Fig. 10C).

Neurocan binds to the related adhesion molecule L1 through the C-terminal sushi domain, which contains about half of the GAG chains present in Neurocan.[17] To assess the role

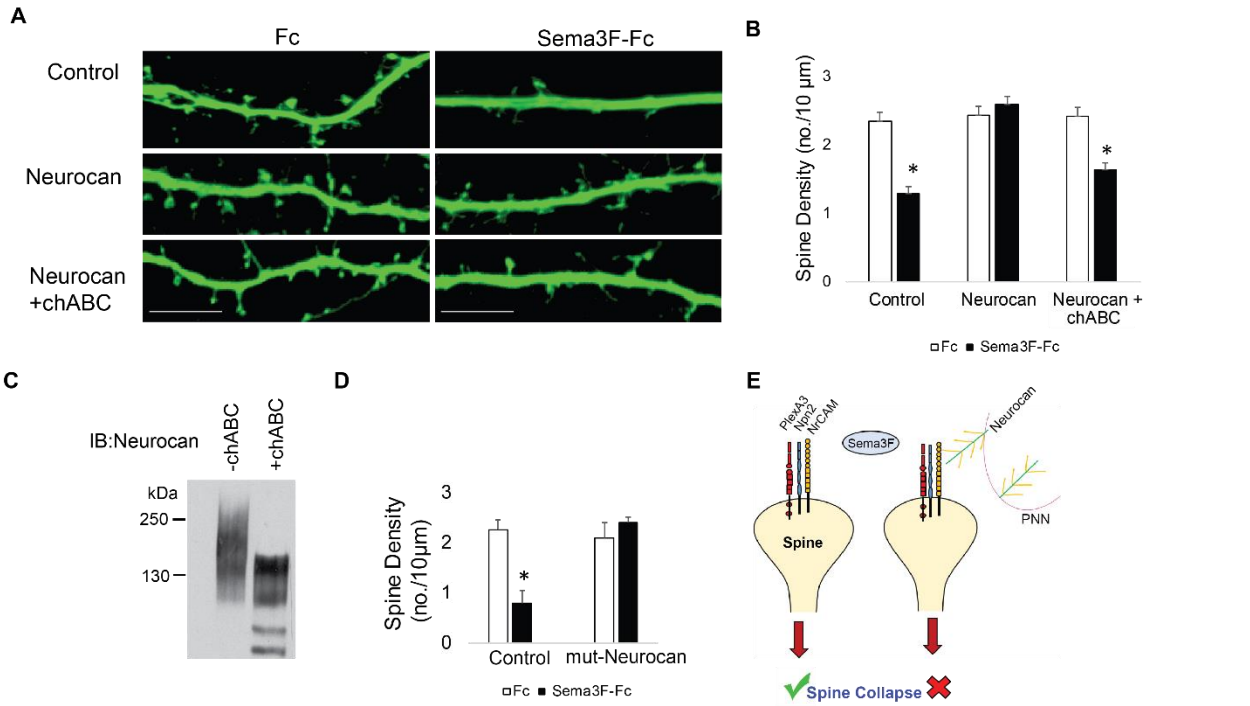

Figure 10: Enzymatic digestion of Neurocan GAG chains with chondroitinase ABC decreases its ability to inhibit Sema3F-induced spine retraction. (A) Images showing spines on apical dendrites from cortical neurons (EGFP, green) in culture treated with Fc or Sema3F-Fc. Neurocan blocked Sema3F-mediated spine retraction, whereas chABC-treated Neurocan was not effective. Scale bar = 10µm. (B) Quantification of experiment in panel A shows a significant reduction in mean spine density of control neurons treated with Sema3F-Fc compared to Fc. Sema3F-induced spine retraction was fully blocked by 20 nM Neurocan, as well as by chABC-digested Neurocan *$p<0.05$, t test; n=3, 10 neurons per condition). (D) Immunoblotting of Neurocan before and after treatment with chABC to remove GAG chains. A shift in apparent molecular size of chABC-treated Neurocan was observed, reflecting a decrease in GAG content. (D) Mouse cortical neurons with and without pre-treatment with recombinant mut Neurocan lacking the C-terminal sushi domain (20 nM, 30 min) showed the mouse Neurocan fragment inhibited Sema3F-Fc induced spine retraction. (E) Model showing that interaction of the PNN protein Neurocan with NrCAM on the surface of dendritic spines in cortical pyramidal neurons terminates Sema3F-induced dendritic spine remodeling during postnatal maturation. Neurocan core protein is depicted in green with yellow GAG chains. The Sema3F receptor complex is comprised of NrCAM (yellow), Npn2 (blue) and PlexA3 (red) subunits.

of the Neurocan sushi domain in NrCAM-mediated spine retraction, a recombinant mouse Neurocan fragment lacking the sushi domain (mutNeurocan) was assayed for inhibition of Sema3F-induced spine retraction in cortical neuron cultures. Neurocan lacking the sushi domain effectively inhibited Sema3F-mediated spine retraction, indicating that NrCAM, unlike L1, does not require the sushi domain or GAG-modification of the sushi region (Fig. 10D).

DISCUSSION

We report here that Neurocan, one of the first CSPGs to be expressed in the maturing neocortex[18] is expressed coordinately with Sema3F in postnatal and adult mouse brain in close apposition to dendritic spines and axon terminals. Neuronal spine retraction and cell binding studies showed that Neurocan interacts with NrCAM and inhibits Sema3F-mediated dendritic spine elimination, providing insight into the molecular basis of PNN-mediated restriction of synaptic plasticity. Our results support a model (Fig. 10E) in which NrCAM/Npn2/PlexA3 functions as a holoreceptor complex for Sema3F that prunes excess dendritic spines from pyramidal neuron subpopulations during postnatal stages of active spine remodeling in the cerebral cortex. As PNNs arise during subsequent maturation, Neurocan within the PNN meshwork interacts with NrCAM on dendritic spines to terminate Sema3F-mediated spine pruning.

In postnatally developing areas of the mouse neocortex (MFC and V1), Neurocan was localized around processes, spines, and soma of Nex1-expressing postmitotic pyramidal neurons, then declined to lower levels in adulthood. As shown by immuno-electron microscopy of the frontal cortex (P18), Neurocan was prominent at plasma membranes and extracellular space, often in proximity to spines, axon terminals, and postsynaptic densities. Previously, we showed that Neurocan was also localized to perisomatic axon terminals and soma of inhibitory interneurons in the MFC.[3] The present findings are in agreement with PNN localization at the surface of pyramidal cells in adult rat V1 and MFC[19] and near dendritic spines in mouse hippocampus. In a functional assay for Sema3F signaling in cortical neuron cultures, we found that Neurocan inhibited spine retraction on apical dendrites of pyramidal neurons. Similarly, in a model cell assay for Sema3F-induced repulsion, Neurocan inhibited morphological retraction

through Sema3F receptor subunits NrCAM, Npn2, and PlexA3. Our culture experiments are in accord with two-photon live imaging studies in adult mouse visual cortex, which demonstrated that CSPGs inhibited spine dynamics and constrained spine morphology, and these effects were reversed by GAG chain degradation.[14,16] The present findings suggest that Neurocan, possibly in conjunction with other CSPGs may contribute to terminating the highly active spine remodeling of juvenile cortical pyramidal neurons during the transition to adulthood.

Cell binding and ELISA assays showed that Neurocan was able to bind NrCAM within its extracellular region, which engages in homophilic and heterophilic interactions. chABC perturbed the ability of Neurocan to block Sema3F-mediated spine pruning in cultured neurons, indicating that GAG chains mediated this inhibition. Our binding results with recombinant proteins support radioimmunoassay studies showing binding of full length NrCAM purified from mouse brain to Neurocan.[8,20] Our experiments with the NrCAM extracellular domain protein fused to Fc further demonstrate that Neurocan interacts with the extracellular region of NrCAM sufficiently to impair neuronal function.

A limitation of the present work is that it is not known how NrCAM association with Neurocan inhibits spine remodeling, such as by altering upstream interactions or downstream signaling. Our results clearly showed that Neurocan did not interact with the upstream ligand Sema3F. Unlike Sema3A, which associates with the CSPGs versican and aggrecan in the brain extracellular matrix.[21] Sema3F-Fc did not bind purified Neurocan, thus upstream sequestration of Sema3F is unlikely be responsible for inhibiting spine remodeling. We recently reported that NrCAM, Npn2, and PlexA3 form a complex for Sema3F required for spine retraction.[2] Neurocan binding might alter the conformation of NrCAM within the holoreceptor complex to prevent Sema3F-induced changes in receptor function. Such an alteration could be subtle, because

Neurocan did not perturb the ability of NrCAM to co-immunoprecipitate with Npn2 from transfected HEK293 cells (not shown). The carboxy-terminal sushi domain of Neurocan, which mediates binding to L1-CAM[17] was dispensable for inhibiting NrCAM-dependent spine retraction, suggesting a different mode of binding to NrCAM. Currently, little is known about Sema3F-induced signaling through PlexA3 in dendritic spines, future studies will be needed to address the possibility that Neurocan influences downstream pathways.

Neurocan and other CSPGs in PNNs have been reported to associate with Ig-class adhesion molecules, including NCAM, L1, NgCAM, Neurofascin, and TAG1, as well as integrins.[8,17,22,23] Thus, Neurocan could have multiple targets in developing neurons, some of which may contribute to spine remodeling. For example, an inhibitory role for Neurocan was recently identified in terminating postnatal remodeling of GABAergic axon terminals in prefrontal cortex to stabilize perisomatic inhibitory synapses.[3] Neurocan binds the NCAM Ig2 domain and competitively inhibits NCAM-EphA3 association to prevent ephrinA5/EphA3 signaling and axonal repulsion.

An inhibitory function of Neurocan in Sema3F-mediated spine pruning in the adolescent brain, suggested by our *in vitro* studies, might serve to protect a subpopulation of cortical pyramidal neurons from over-pruning of dendritic spines. Other mechanisms of synaptic elimination involve astrocyte-mediated phagocytosis through engulfment receptors (MerTK and MEGF10), microglia-mediated pruning (C1q, C3, and CX3CR1)[24] and autophagy through mTOR signaling.[25] The involvement of Neurocan in regulating synapse remodeling on both excitatory and inhibitory neurons makes it an important candidate molecule for neurodevelopmental disorders with aberrant spine and synapse numbers that could impact cortical excitatory/inhibitory balance. In schizophrenia, PNNs are notably altered in human

prefrontal cortex[26] where dendritic spine density is markedly diminished[27-30] and Neurocan is a candidate locus for schizophrenia, bipolar, and other neurological disorders.[31-34]

In conclusion, we provide evidence that the PNN protein Neurocan acts as a developmental brake for spine remodeling mediated by Sema3F and NrCAM in the maturing mouse neocortex.

REFERENCES

Agarwal A., Dibaj P., Kassmann C. M., Goebbels S., Nave K. A., Schwab M. H. (2012). In vivo imaging and noninvasive ablation of pyramidal neurons in adult NEX-CreERT2 mice. *Cereb. Cortex* 22 1473–1486.

Mohan V., Sullivan C. S., Guo J., Wade S. D., Majumder S., Agarwal A., et al. (2018). Temporal regulation of dendritic spines through NrCAM-semaphorin3f receptor signaling in developing cortical pyramidal neurons. *Cereb. Cortex*

Sullivan C. S., Gotthard I., Wyatt E. V., Bongu S., Mohan V., Weinberg R. J., et al. (2018). Perineuronal net protein neurocan inhibits NCAM/EphA3 repellent signaling in GABAergic interneurons. *Sci. Rep.* 8:6143.

Shen Y., Tenney A. P., Busch S. A., Horn K. P., Cuascut F. X., Liu K., et al. (2009). PTPsigma is a receptor for chondroitin sulfate proteoglycan, an inhibitor of neural regeneration. *Science* 326 592–596.

Flanagan J. G., Cheng H. J. (2000). Alkaline phosphatase fusion proteins for molecular characterization and cloning of receptors and their ligands. *Methods Enzymol.* 327 198–210.

Peng S. S., Tran T. S. (2017). Regulation of cortical dendrite morphology and spine organization by secreted semaphorins: a primary culture approach. *Methods Mol. Biol.* 1493 209–222.

Friedlander D. R., Milev P., Karthikeyan L., Margolis R. K., Margolis R. U., Grumet M. (1994). The neuronal chondroitin sulfate proteoglycan Neurocan binds to the neural cell adhesion molecules Ng-CAM/L1/NILE and N-CAM, and inhibits neuronal adhesion and neurite outgrowth. *J. Cell Biol.* 125 669–680.

Milev P., Chiba A., Haring M., Rauvala H., Schachner M., Ranscht B., et al. (1998). High affinity binding and overlapping localization of neurocan and phosphacan/protein-tyrosine phosphatase-zeta/beta with tenascin-R, amphoterin, and the heparin-binding growth-associated molecule. *J. Biol. Chem.* 273 6998–7005.

Rauch U., Karthikeyan L., Maurel P., Margolis R. U., Margolis R. K. (1992). Cloning and primary structure of neurocan, a developmentally regulated, aggregating chondroitin sulfate proteoglycan of brain. *J. Biol. Chem.* 267 19536–19547.

Bhattacharyya S., Zhang X., Feferman L., Johnson D., Tortella F. C., Guizzetti M., et al. (2015). Decline in arylsulfatase B and Increase in chondroitin 4-sulfotransferase combine to increase chondroitin 4-sulfate in traumatic brain injury. *J. Neurochem.* 134 728–739.

Turner L. J., Hall A. (2006). Plexin-induced collapse assay in COS cells. *Methods Enzymol.* 406: 665–676.

Carulli D., Foscarin S., Faralli A., Pajaj E., Rossi F. (2013). Modulation of semaphorin3A in perineuronal nets during structural plasticity in the adult cerebellum. *Mol. Cell. Neurosci.* 57 10–22.

Dick G., Tan C. L., Alves J. N., Ehlert E. M., Miller G. M., Hsieh-Wilson L. C., et al. (2013). Semaphorin 3A binds to the perineuronal nets via chondroitin sulfate type E motifs in rodent brains. *J. Biol. Chem.* 288 27384–27395.

Pizzorusso T., Medini P., Berardi N., Chierzi S., Fawcett J. W., Maffei L. (2002). Reactivation of ocular dominance plasticity in the adult visual cortex. *Science* 298 1248–1251.

Orlando C., Ster J., Gerber U., Fawcett J. W., Raineteau O. (2012). Perisynaptic chondroitin sulfate proteoglycans restrict structural plasticity in an integrin-dependent manner. *J. Neurosci.* 32 18009–18017, 18017a.

de Vivo L., Landi S., Panniello M., Baroncelli L., Chierzi S., Mariotti L., et al. (2013). Extracellular matrix inhibits structural and functional plasticity of dendritic spines in the adult visual cortex. *Nat. Commun.* 4:1484.

Oleszewski M., Gutwein P., Von Der Lieth W., Rauch U., Altevogt P. (2000). Characterization of the L1-neurocan-binding site. Implications for L1-L1 homophilic binding. *J. Biol. Chem.* 275 34478–34485.

Carulli D., Pizzorusso T., Kwok J. C., Putignano E., Poli A., Forostyak S., et al. (2010). Animals lacking link protein have attenuated perineuronal nets and persistent plasticity. *Brain* 133 2331–2347.

Alpar A., Gartner U., Hartig W., Bruckner G. (2006). Distribution of pyramidal cells associated with perineuronal nets in the neocortex of rat. *Brain Res.* 1120 13–22.

Grumet M., Sakurai T. (1996). Heterophilic interactions of the neural cell adhesion molecules Ng-CAM and Nr-CAM with neural receptors and extracellular matrix proteins. *Semin. Neurosci.* 8 379–389.

Vo T., Carulli D., Ehlert E. M., Kwok J. C., Dick G., Mecollari V., et al. (2013). The chemorepulsive axon guidance protein semaphorin3A is a constituent of perineuronal nets in the adult rodent brain. *Mol. Cell. Neurosci.* 56 186–200.

Falk J., Thoumine O., Dequidt C., Choquet D., Faivre-Sarrailh C. (2004). NrCAM coupling to the cytoskeleton depends on multiple protein domains and partitioning into lipid rafts. *Mol. Biol. Cell* 15 4695–4709.

Hedstrom K. L., Xu X., Ogawa Y., Frischknecht R., Seidenbecher C. I., Shrager P., et al.

(2007). Neurofascin assembles a specialized extracellular matrix at the axon initial segment. *J. Cell Biol.* 178 875–886.

Chung W. S., Welsh C. A., Barres B. A., Stevens B. (2015). Do glia drive synaptic and cognitive impairment in disease? *Nat. Neurosci.* 18 1539–1545.

Huber K. M., Klann E., Costa-Mattioli M., Zukin R. S. (2015). Dysregulation of mammalian target of rapamycin signaling in mouse models of Autism. *J. Neurosci.* 35 13836–13842.

Berretta S., Pantazopoulos H., Markota M., Brown C., Batzianouli E. T. (2015). Losing the sugar coating: potential impact of perineuronal net abnormalities on interneurons in schizophrenia. *Schizophr. Res.* 167 18–27.

Garey L. J., Ong W. Y., Patel T. S., Kanani M., Davis A., Mortimer A. M., et al. (1998). Reduced dendritic spine density on cerebral cortical pyramidal neurons in schizophrenia. *J. Neurol. Neurosurg. Psychiatry* 65 446–453.

Glausier J. R., Lewis D. A. (2013). Dendritic spine pathology in schizophrenia. *Neuroscience* 251 90–107. 10.1016/j.neuroscience.2012.04.044

MacDonald M. L., Alhassan J., Newman J. T., Richard M., Gu H., Kelly R. M., et al. (2017). Selective loss of smaller spines in Schizophrenia. *Am. J. Psychiatry* 174 586–594.

Moyer C. E., Shelton M. A., Sweet R. A. (2015). Dendritic spine alterations in schizophrenia. *Neurosci. Lett.* 601 46–53.

Cichon S., Muhleisen T. W., Degenhardt F. A., Mattheisen M., Miro X., Strohmaier J., et al. (2011). Genome-wide association study identifies genetic variation in neurocan as a susceptibility factor for bipolar disorder. *Am. J. Hum. Genet.* 88 372–381.

Muhleisen T. W., Mattheisen M., Strohmaier J., Degenhardt F., Priebe L., Schultz C. C., et al. (2012). Association between schizophrenia and common variation in neurocan (NCAN), a genetic risk factor for bipolar disorder. *Schizophr. Res.* 138 69–73.

Schultz C. C., Muhleisen T. W., Nenadic I., Koch K., Wagner G., Schachtzabel C., et al. (2014). Common variation in NCAN, a risk factor for bipolar disorder and schizophrenia, influences local cortical folding in schizophrenia. *Psychol. Med.* 44 811–820.

Wang P., Cai J., Ni J., Zhang J., Tang W., Zhang C. (2016). The NCAN gene: schizophrenia susceptibility and cognitive dysfunction. *Neuropsychiatr. Dis. Treat.* 12 2875–2883.

APPENDIX ONE: PERINEURONAL NET PROTEIN NEUROCAN INHIBITS NCAM/EphA3 REPELLENT SIGNALING IN GABAERGIC INTERNEURONS[1]

INTRODUCTION

Perineuronal nets (PNNs) are implicated in closure of critical periods of synaptic plasticity in the brain, but the molecular mechanisms by which PNNs regulate synapse development remain obscure. A receptor complex of NCAM and EphA3 mediates postnatal remodeling of inhibitory perisomatic synapses of GABAergic interneurons onto pyramidal cells in the mouse frontal cortex necessary for excitatory/inhibitory balance. Here it is shown that enzymatic removal of PNN glycosaminoglycan chains decreased the density of GABAergic perisomatic synapses in mouse organotypic cortical slice cultures. Neurocan, a key component of PNNs, was expressed in postnatal frontal cortex in apposition to perisomatic synapses of parvalbumin-positive interneurons. Polysialylated NCAM (PSA-NCAM), which is required for ephrin-dependent synapse remodeling, bound less efficiently to neurocan than mature, non-PSA-NCAM. Neurocan bound the non-polysialylated form of NCAM at the EphA3 binding site within the immunoglobulin-2 domain. Neurocan inhibited NCAM/EphA3 association, membrane clustering of NCAM/EphA3 in cortical interneuron axons, EphA3 kinase activation, and ephrin-A5-induced growth cone collapse. These studies delineate a novel mechanism wherein neurocan inhibits NCAM/EphA3 signaling and axonal repulsion, which may terminate postnatal remodeling of interneuron axons to stabilize perisomatic synapses *in vivo*.

[1] This chapter previously appeared as an article in the journal Scientific Reports. The author contributed to immunofluorescence staining and pull-down binding experiments. The original citation is as follows: Sullivan CS, Gotthard I, Wyatt EV, Bongu S, Mohan V, Weinberg RJ, Maness PF. (2017) Perineuronal net protein Neurocan inhibits NCAM/EphA3 repellant signaling in GABAergic interneurons. *Scientific Reports.* 8(1):6143.

MATERIALS AND METHODS

Mice

Mice were used according to the University of North Carolina Institutional Animal Care and Use Committee (IACUC) policies (AAALAC Institutional Number: #329) and in accordance with NIH guidelines, and all animal protocol procedures were approved by the University of North Carolina IACUC (IACUC ID# 15-243). The *Pvalb*-IRES-Cre line[1] (JAX No. 008069) was crossed to the Ai9 reporter line[2] (JAX No. 007909) to label cells with tdTomato after Cre-mediated recombination. Mice were maintained on the C57BL/6 background.

Immunochemicals and reagents

Monoclonal antibodies used were directed against NCAM (OB11; Sigma Aldrich), phosphotyrosine (PY99; Santa Cruz Biotechnology), versican (sc-47769, Santa Cruz Biotechnology), C-4-S (MAB2030, Millipore Sigma), and PSA (Ab5324, Millipore). An antibody recognizing a shared epitope of aggrecan and brevican (sc-166951, Santa Cruz Biotechnology) was also used. Polyclonal antibodies were against neurocan (AF5800, R&D), EphA3 (C-19; Santa Cruz Biotechnology), NCAM (H300; Santa Cruz Biotechnology), GAPDH (IMG-3073, Imgenex), GABA (A2052; Sigma and ab17413; Abcam), GAD65 (GAD-6; Developmental Studies Hybridoma Bank), MATH-2 (ab85824; Abcam), and GFP (13970; Abcam). Normal rabbit IgG and goat anti-human IgG were from Jackson ImmunoResearch Laboratories. Secondary antibodies from Life Technologies were antimouse Alexa-488, anti-mouse Alexa-555, anti-mouse Alexa-647, anti-rabbit Alexa-555, and anti-rabbit Alexa-647. Other secondary antibodies used were anti-guinea pig Alexa-405 (Sigma Aldrich), anti-rabbit Alexa-405 (Abcam), anti-human IgG-HRP (Sigma-Aldrich), anti-mouse-HRP (Pierce), anti-goat-HRP (Southern Biotech), and donkey anti-rabbit HRP (Sigma-Aldrich). Labeling of PNNs

was performed using biotinylated *Wisteria Floribunda* Agglutinin (WFA) (L1766; Sigma) and streptavidin-Alexa-647 (S32357; ThermoFisher). Recombinant ephrin-A5-Fc, human Fc, mouse neurocan, human neurocan, and human tenascin-R (R&D Systems) were also used. Human NCAM-Fc proteins[3] were purified from transfected HEK293T cell conditioned media using Protein A Sepharose (Pierce). Chondroitinase ABC and penicillinase were purchased from Sigma Aldrich. Endoneuraminidase-N (endo-N), which removes α-2,8 sialic acid chains,[4] was a gift of Urs Rutishauser (Memorial Sloan-Kettering Cancer Center).

Enzymatic treatment of organotypic brain slices

Organotypic slice cultures containing the PFC were prepared by sectioning the brain of PV-Cre;Ai9 mice at age P5 in the coronal plane (400 μm).[5] Slices were cultured in Millicell tissue culture inserts in Dulbecco's Modified Eagle's Media (DMEM) containing 20% horse serum, 1 mM L-glutamine, 13 mM D-glucose, 1 mM $CaCl_2$, 2 mM $MgSO_4$, 1 μg/mL insulin, 30 mM HEPES, 5 mM $NaHCO_3$, and 0.001% ascorbic acid, which was replaced every 2 days as described.[6] Slices at 12 days *in vitro* (DIV) were treated with chABC (0.2U/mL) or control penicillinase (0.2U/ml) for 2 hours,[7] followed by 2 rinses with culture media to remove enzyme and another 2 days of culture before fixation on DIV14. Slices were fixed in 4% PFA and stained with antibodies to NeuN to mark neuronal nuclei (1:400),[8] tdTomato to label perisomatic puncta (1:100), and biotinylated WFA to label PNNs (1:500) followed by detection with streptavidin-Alexa647. A blinded observer scored the average number of perisomatic puncta within 2 μm of NeuN-labeled nuclei from 3 animals per enzymatic treatment condition (30 cells/condition). The efficiency of chABC treatment was verified by imaging WFA labeling compared to the control condition (penicillinase-treated). For rescue experiments, slices were treated with enzyme at DIV 12 for 2 hours, rinsed twice with culture media, and then cultured in media containing no added

protein (control untreated), recombinant neurocan (20 μg/ml), or recombinant tenascin-R (20 μg/ml) until fixation on DIV 14.

Electron microscopy and immunogold labeling

C57BL/6 WT mice were anesthetized and perfused transcardially with phosphate buffered saline (PBS) followed by 4% PFA + 0.1% glutaraldehyde in PBS. Brains were postfixed for 2 days in the same fixative, and 50 μm thick coronal sections were cut using a vibratome. Pre-embedding immunogold labeling with silver enhancement was performed for neurocan. To quench glutaraldehyde, sections were pretreated with 1% $NaBH_4$ in PBS and then 3% H_2O_2 in PBS, followed by blocking in 10% normal donkey serum. Sections were incubated overnight in primary antibody diluted at 1:500-1:2000 in PBS, rinsed, briefly re-blocked in 2% normal donkey serum, and incubated for 2 hours in biotinylated donkey anti-sheep secondary (Jackson ImmunoResearch 713-065-147). Samples were rinsed and incubated 1 hour in streptavidin-nanogold (Nanoprobes 2016) at 1:100 in 1% normal donkey serum/PBS. Sections were stabilized in 2% glutaraldehyde/PBS for 30' and then rinsed in PBS followed by 0.05 M sodium acetate. After transfer to new vials, sections were silver-enhanced for 7' using HQ silver enhancement kit (Nanoprobes 2012), rinsed with 0.05 M sodium acetate, and moved to phosphate buffer, pH 6.8. Sections for electron microscopy were then post-fixed 45' in 0.5% osmium tetroxide in phosphate buffer, pH 6.8, rinsed, and placed in 0.1 M maleate buffer, pH 6, followed by 45' in 1% uranyl acetate/MB. Sections were dehydrated through a graded ethanol series ending with 2 changes of 100% ethanol. Resin infiltration was 30' in 1:1 ethanol/resin, 30' 1:3 ethanol/resin, then 2 changes in pure resin (Low Viscosity embedding kit—from Dr. Spurr, Electron Microscopy Sciences 14300). Infiltrated sections were sandwiched between 2 strips of ACLAR film (between 2 glass slides for support) and polymerized for 36-48 hours in an oven.

Small (1x1mm) areas of interest from neocortex were cut out and glued onto a support block. The tissue was trimmed and sectioned (50-60 nm) (Leica Ultracut R) and sections collected on 300 mesh nickel or copper grids. Tissue sections were then counterstained with uranyl acetate followed by Sato's lead and examined with a Tecnai 12 electron microscope.

Immunoprecipitation and pull-down assays

For coimmunoprecipitation of neurocan with NCAM140, NCAM mutants, or EphA3, HEK293T cells (cultured in DMEM, 10% fetal bovine serum) were transfected with EphA3 or NCAM140 cDNA (in pcDNA3.1 vectors) using Lipofectamine 2000 (Invitrogen). Proteins from cell lysates (1 mg) in RIPA buffer (20 mM Tris pH 7.0, 0.15 M NaCl, 5 mM ethylenediaminetetraacetic acid (EDTA), 1 mM EGTA, 1% NP-40, 1% deoxycholate, 0.1% sodium dodecyl sulfate (SDS), 200 μM Na_3VO_4, 10 mM NaF, 1X protease inhibitor (Sigma)), and proteins were precipitated using antibodies against EphA3 (C-19, Santa-Cruz), or NCAM (H-300 Santa-Cruz), with Protein A/G agarose beads (Thermo-Fisher). Co-immunoprecipitation from brain was performed using 1 mg of lysate in RIPA buffer. In some experiments, brain extracts were treated for 1 hr with endo-N (40 U) on ice prior to immunoprecipitation to remove PSA.[5] Protein complexes were separated by SDS-polyacrylamide gel electrophoresis (SDS-PAGE), immunoblotted using antibodies to versican, aggrecan/brevican, neurocan, EphA3, NCAM, or phosphotyrosine, and detected with HRP-conjugated secondary antibodies. Pulldown analyses were performed by incubating 1 μg of neurocan (human or mouse) with Fc protein (1 μg) (control Fc, NCAM-EC-Fc, NCAM Ig1-3, NCAM Ig1-2, NCAM Ig2, NCAM Ig1, or ephrin-A5-Fc) in TBS for 1 hr at 37°C. Protein A/G Sepharose beads were used to pull down Fc proteins for detection by immunoblotting. For detection of EphA3 autophosphorylation,

HEK293T cells were cotransfected with NCAM-140 and EphA3 cDNA. Transfected cells were pre-treated with neurocan (20 nM) for 30 min prior to
treatment with preclustered ephrin-A5-Fc or control Fc for 10 min,[9] then lysed in RIPA buffer. EphA3 was immunoprecipitated, and tyrosine phosphorylation was detected with anti-PY99.

Competitive binding assay

HEK293T cells were transfected with NCAM-140 and EphA3. Recombinant neurocan was treated with 0.1 U/microgram chABC (Sigma) at 37°C for 1.5 hr or incubated with no enzyme (as a control), followed by heat inactivation of enzyme at 100°C for 10 min. Efficacy of chABC treatment was assessed by immunoblotting. Cells were treated with neurocan (20 nM), chABC treated neurocan (20 nM), or no neurocan (control) for 30 min. Cells were lysed and NCAM immunoprecipitated, and bound EphA3 and neurocan were detected by immunoblotting.

Immunostaining and co-localization analysis

For cortical neuron cultures, embryonic day 0.5 (E0.5) was defined as the plug date and cortical neuron cultures prepared at E15.5. Dissociated cortical neurons from WT mice were plated onto poly-D-lysine- and laminin coated Lab-Tek II chamber slides ($1.5\times 10_5$ cells/well) as described.[10,11] At 10 DIV, cells were pretreated with or without neurocan (4 nM) and then stimulated with 1 μg/mL preclustered Fc or ephrin-A5-Fc for 30 min. Cells were fixed in 4% paraformaldehyde and blocked/permeabilized in 0.5% TritonX-100/PBS with 10% horse serum. Slides were incubated in primary antibodies against NCAM, EphA3, and GABA overnight at 4°C. Secondary antibodies (Alexa 405, Alexa 555, Alexa 647) were added for 1 hr and mounted using SlowFade (Life Technologies). Confocal images were obtained with Zeiss LSM700 and LSM710 microscopes using a Plan-Apochromat 63X 1.4 numerical aperture objective with 2X optical zoom using Zeiss Zen software. Only GABA-positive cells were imaged for analysis. Co-

localization of NCAM and EphA3 was analyzed using the ImageJ plugins Colocalization_Test and Colocalization Threshold as described previously.[12] Co-localization was expressed as R-Total (the Pearson correlation coefficient, which varies between -1 and 1). Values were calculated for pixels above a threshold level determined by the regression algorithm contained in the "Colocalization Threshold" macro. For each condition, an average from measurements of at least 30 images was reported.

Growth cone collapse assay

Dissociated cortical neuron cultures were generated from WT mice as described above. At 10 DIV, cells were pre-treated with or without neurocan (4 nM) and then with preclustered ephrin-A5-Fc or human Fc (1 μg/mL) for 30 min, fixed, and growth cones visualized by immunofluorescence staining of GABA.[5,12] Growth cones were scored as collapsed by bullet-shaped morphology or noncollapsed by spread morphology by an observer blinded to treatment, and the percentage of collapsed growth cones of GABA-positive neurons was compared (10 fields/well; ≥ 2 wells/experiment; ≥ 300 growth cones/condition).

RESULTS

Degradation of PNN GAG chains reduces perisomatic synapse density in cortical slices

To directly test the importance of PNN molecules in regulation of perisomatic GABAergic synapse density in the PFC, organotypic slice cultures were prepared from Parvalbumin-Cre;Ai9 (Lox-STOP-Lox tdTomato) mice, in which parvalbumin-positive interneurons express tdTomato throughout the soma and neuronal processes as a reporter of Cre-dependent recombination.[1,2] Interneurons in the PFC in these slice cultures form characteristic axon arbors and perisomatic boutons over 14 days *in vitro* (DIV)[5] with a time course analogous to that observed *in vivo.*[11] We focused on the anterior cingulate region of the PFC (layers 2,3), because it is a region where synaptic plasticity is pronounced and intra- and subcortical inputs are maximal.[13,14] *Wisteria Floribunda* agglutinin (WFA) is a lectin that binds to residues found within PNN GAG chains.[15] WFA labeling of PNNs in layers 2,3 of the anterior cingulate at 14 DIV showed characteristic PNNs around populations of NeuN-positive neuronal soma, as well as tdTomato-labeled interneurons (Fig. 11A).

To determine if GAG-modified PNNs restrained postnatal remodeling of perisomatic basket cell synapses, slice cultures (DIV12) were treated with a control enzyme (penicillinase) or the bacterial enzyme chondroitinase ABC (chABC) for 2 hours, followed by removal of enzyme and further incubation until fixation at DIV14 (equivalent postnatal day 19). Penicillinase is a bacterial-derived enzyme that is used as a non-relevant control for comparison to chABC.[16] chABC treatment was sufficient to remove PNNs as indicated by a loss of WFA staining in the chABC treated slices (Fig. 11B). Treatment with chABC significantly decreased the mean number of perisomatic puncta per soma in comparison to control penicillinase, implicating PNN proteins as a stabilizing factor for perisomatic synapses (Fig. 11C,D). Neurocan coimmunoprecipitated with NCAM in brain lysates (Fig. 11E), and previous work indicates that

purified NCAM and neurocan can associate in a partially GAG-dependent manner *in vitro.*[17] Chondroitinase ABC will target the GAG chains of neurocan and other CSPGs in PNNs. However, NCAM did not bind other CSPG proteins (versican, aggrecan, brevican), as shown by lack of co-immunoprecipitation from brain lysates (Fig. 11E). Although NCAM can bind the CSPG phosphacan, this depends on the core protein rather than GAG chains.[18]

Although our chABC results in organotypic slices suggested that PNN components may regulate perisomatic synapses, no specific target of chABC in this process was identified. We hypothesized that neurocan may regulate perisomatic synapses based on its binding to NCAM. However, chABC treatment has also been shown to reduce tenascin-R,[19] a PNN glycoprotein that contributes to formation and activity of perisomatic GABAergic interneurons in the CA1 area of the hippocampus.[20-23] Thus, we wanted to identify whether neurocan and/or tenascin-R were involved in setting the number of perisomatic GABAergic synapses in organotypic slices. To assess the role of these proteins in regulation of perisomatic synapses, we performed a rescue experiment in which organotypic slices were treated with control penicillinase or chABC (DIV 10, 2 hours) followed by removal of enzyme and addition of no protein (untreated), neurocan, or tenascin-R. Rescue with recombinant neurocan but not tenascin-R prevented the decrease of perisomatic synapses previously observed after chABC treatment (Fig. 11F). However, further testing of the recombinant tenascin-R protein for the presence of HNK-1 carbohydrate modification indicated that the protein lacked detectable HNK-1 (Fig. 11G). HNK-1 modification has been shown to be required for the synaptogenic effects of tenascin-R.[20-23] The rescue experiment with recombinant neurocan indicates that neurocan but not tenascin-R lacking HNK-1 is sufficient to rescue perisomatic innervation after chABC.

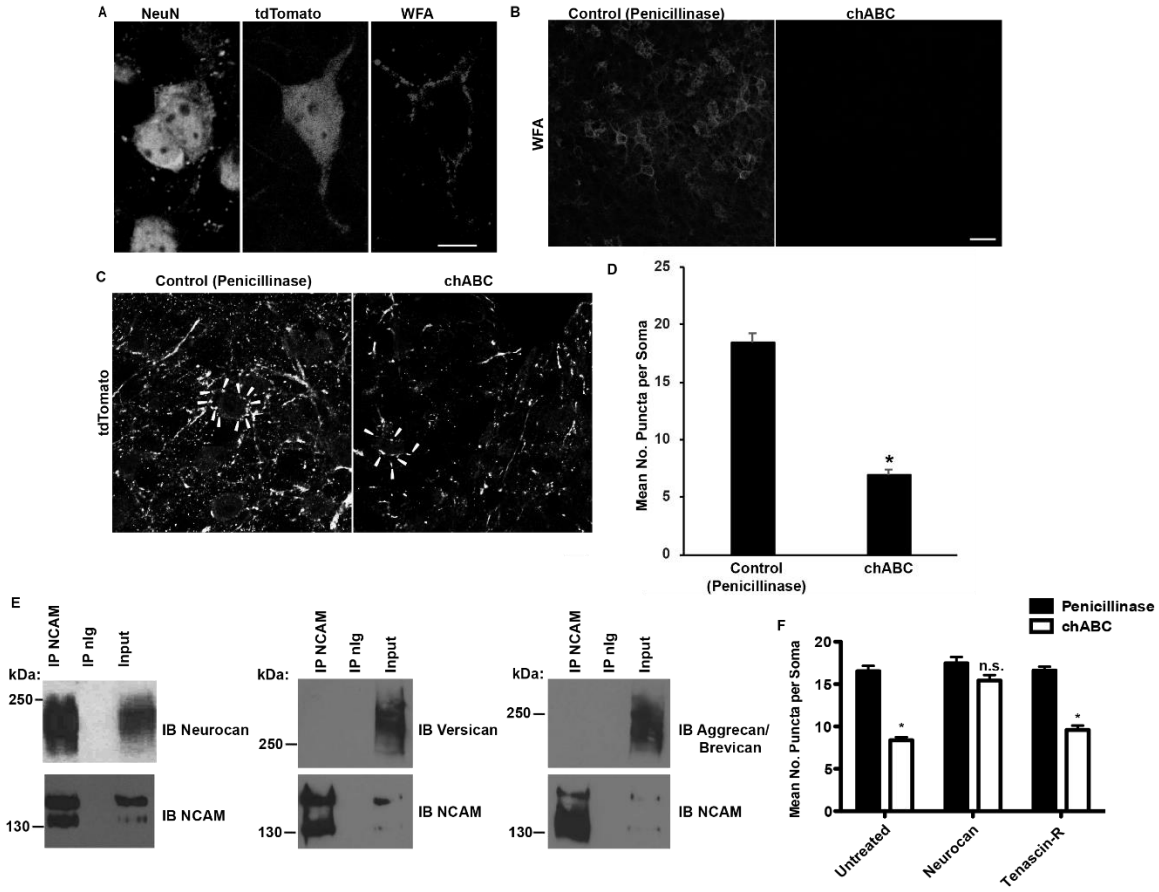

Figure 11: GAG-modified neurocan blocks chABC-induced decrease of perisomatic synaptic puncta in organotypic brain slices. (A) Immunostaining of neuronal soma (NeuN), a parvalbumin-positive interneuron (tdTomato), and a perineuronal net (WFA) in DIV14 organotypic brain slice culture. Scale bar=10 μm. (B) WFA labeling of perineuronal nets in control penicillinase and chABC-treated brain slices. Scale bar=30 μm. (C) Representative image of perisomatic synapses (tdTomato) in control penicillinase or chABC-treated slice cultures. Representative perisomatic puncta around a single soma are indicated with arrowheads. Scale bar= 10 μm. (D) Quantification of the mean number of perisomatic synaptic puncta per soma (n=30 soma/condition, 3 animals per condition, t-test, * $p<0.05$). (E) NCAM was immunoprecipitated from brain lysates, followed by immunoblotting with antibodies against neurocan, versican, or aggrecan/brevican (using an antibody raised against shared epitope). (F) Slices were treated with control penicillinase or chABC as in (C) followed by rescue with neurocan or tenascin-R. Quantification of the mean number of perisomatic synapses per soma 30 was performed (>90 soma per mouse per condition, n=3 mice, two-way ANOVA with Bonferonni post-hoc testing, * $p<0.05$).

Expression of Neurocan and NCAM in the postnatally developing PFC

The temporal and spatial expression of neurocan in the neocortex could affect its function in specific cell types or brain circuits. Neurocan was found to be prominently expressed in mouse brain at birth (postnatal day zero, P0), increased at early postnatal and adolescent stages (P10-P21), and decreased at adulthood (P60) (Fig. 12A), similar to previous results in rat brain.[24] Neurocan was observed as a diffuse protein (130–250 kDa) on immunoblots due to GAG chain

modification. NCAM exhibited a similar developmental pattern of expression as neurocan and displayed regulated changes in polysialylation. NCAM was evident at P0-P21 as a high molecular weight (180–250 kDa) diffuse species that was recognized by PSA-specific antibodies (Fig. 12A). In young adults at P60 NCAM resolved into non-PSA NCAM isoforms of 180- and 140-kDa, which differ only in the length of their cytoplasmic domains[25] (Fig. 12A).

The cellular localization of neurocan in the PFC was next evaluated by immunofluorescence staining in Parvalbumin-Cre;Ai9 reporter mice at P28 (immature) and P60 (adult) (Fig. 12B). In the PFC of these mice, perisomatic puncta of TdTomato-positive basket cells co-localized with GAD65, a presynaptic marker enriched in GABAergic nerve terminals (Fig. 12B). Neurocan was abundant and diffusely localized throughout PFC laminae at P28, and decreased by P60 (Fig. 12C). Somata of many tdTomato-positive interneurons were distinctly outlined by neurocan immunofluorescence (9% and 17% at P28 and P60, respectively) (Fig. 12C). Neurocan localization around pyramidal cells was validated by double immunostaining with the nuclear transcription factor MATH-2, which is specific for pyramidal neurons (Fig. 12D).[26] Neurocan staining was observed within approximately 1 μm of 81% of tdTomato-positive perisomatic puncta around MATH-2-expressing pyramidal cells (Fig. 12D) (n = 3 mice, 150 tdTomato puncta, SEM = 6%). Neurocan localization in the PFC (P18) was further probed at the electron microscope level by immunogold labeling. Neurocan labeling was observed at discrete sites along the somal membrane as well as in the extracellular space adjacent to soma (arrows, Fig. 12E). Neurocan labeling was sometimes seen at the somal membrane in proximity to synaptic vesicle-containing axon terminals (AT, open arrowhead; Fig. 12F), but was rarely seen within the cytoplasm. To verify the specificity of the neurocan antibody, COS7 cells were transfected to express neurocan fused to alkaline phosphatase (Neurocan-AP), or alkaline

phosphatase (AP) alone. Fixed cells were subjected to indirect immunoperoxidase staining with or without neurocan antibodies (Fig. 12G). Only cells expressing Neurocan-AP were positive for labeling. The AP transfected cells and control lacking primary antibody showed no signal, indicating specificity of the antibody. To assess the spatial relationship of neurocan and NCAM in both pyramidal neurons and inhibitory GABAergic interneurons, cortical neuron cultures (14DIV) were stained with antibodies against GABA, NCAM, and neurocan (Fig. 12H). Results indicated that both GABA-positive interneurons and GABA-negative neurons express NCAM and neurocan at neuronal soma (Fig. 12H). Together, these results showed that neurocan was preferentially localized in postnatally developing PFC near neuronal soma membranes and was present around both excitatory and inhibitory neurons.

NCAM polysialylation inhibits binding to Neurocan

Polysialylation of NCAM is required for ephrinA-induced repellent responses of GABAergic interneurons.[5] To determine whether neurocan binds differentially to polysialylated NCAM or unmodified NCAM isoforms, NCAM and neurocan association was analyzed by co-immunoprecipitation from brain lysates at P8, when NCAM is heavily polysialylated, and at P34, when only a small portion of NCAM is PSA-modified (Fig. 13A). Neurocan preferentially immunoprecipitated with non-PSA NCAM at P34 compared to PSA-NCAM at P8 (Fig. 13A,B). To determine if PSA removal increased NCAM/neurocan binding, P8 brain lysates were treated with or without endoneuraminidase N (EndoN) to remove PSA, followed by immunoprecipitation of NCAM. EndoN treatment was effective at decreasing NCAM polysialylation, and significantly increased neurocan binding to non-PSA NCAM-180 and NCAM-140 (Fig. 13C,D). These results support the conclusion that neurocan preferentially binds non-PSA NCAM isoforms.

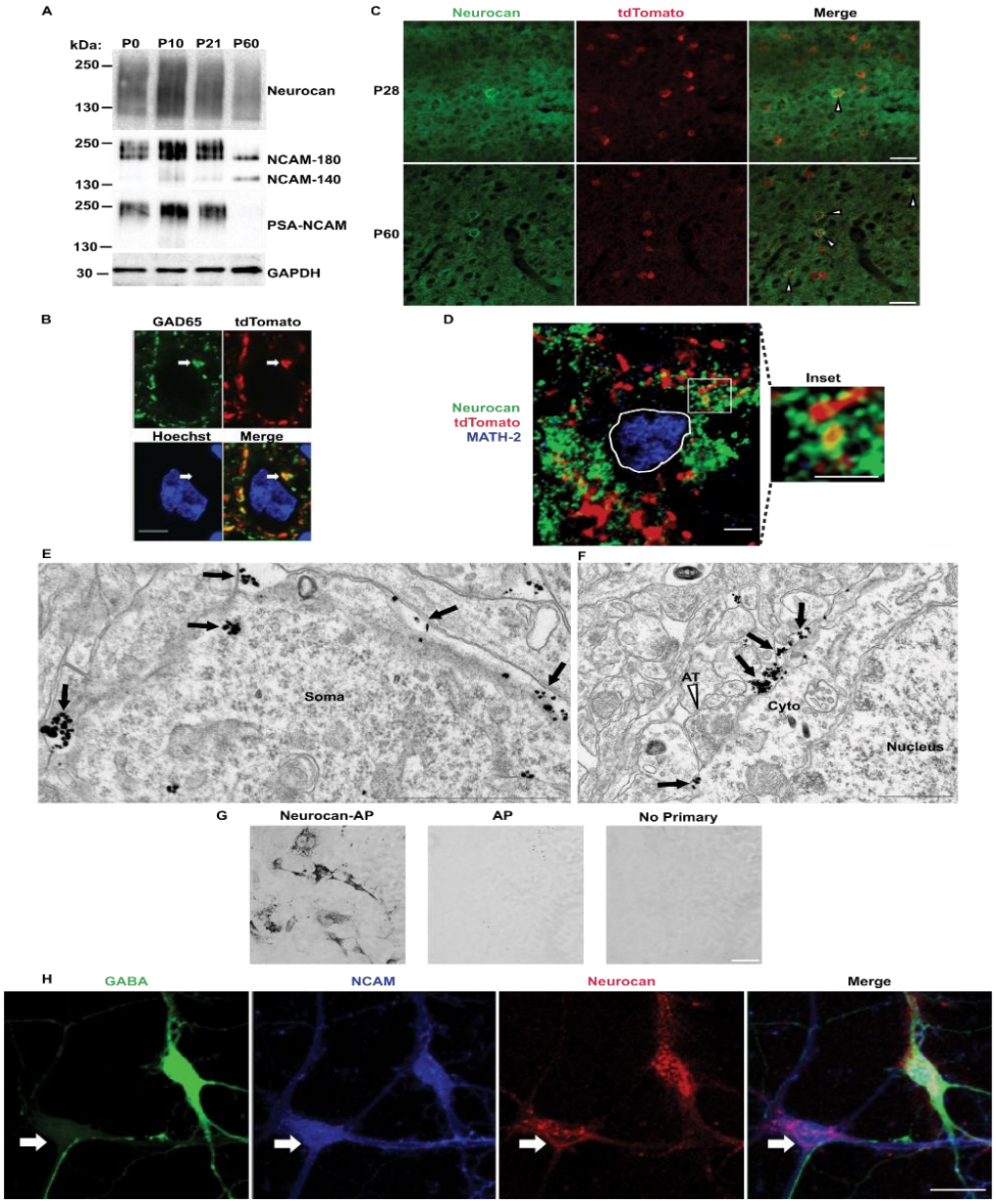

Figure 12: Expression of neurocan and NCAM in postnatal and adult brain. (A) Immunoblot of total brain extracts for neurocan, NCAM, PSA-NCAM, and GAPDH (loading control). (B) Co-localization of tdTomato puncta (red) with the presynaptic marker GAD65 (green) around a neuronal soma (blue). Scale bar=5 μm. (C) Immunofluorescent staining of neurocan (green) around PV+ tdTomato-labeled interneurons (red) in mouse frontal cortex at P28 and P60. Scale bar=50 μm. (D) Confocal images of neurocan (green) around perisomatic synaptic puncta (red) onto MATH-2 expressing pyramidal neurons (blue nucleus, outlined with white border). A magnified inset is indicated with a white box. Scale bars=2.5 μm. (E) Electron micrograph of immunogold labeling for neurocan along the membrane of a neuronal soma (black arrows point to examples). Scale bar=1 μm. (F) Electron micrograph of an inhibitory axon terminal onto a neuronal soma. Neurocan immunogold labeling is indicated with black arrows, and the axon terminal (AT) is labeled with a white arrowhead. Cytoplasm and nucleus of the soma are identified with text. Scale bar=1 μm. (G) Verification of neurocan antibody specificity by immunostaining of COS7 cells transfected with Neurocan-AP (+ control) or AP (- control), and a no primary antibody control. Scale bar=50 μm.(H) Immunofluorescent localization of NCAM and neurocan in GABA+ and GABA- cortical neuron cultures. Confocal images of GABA (green), NCAM (blue), and neurocan (red) in cortical neuron cultures. White arrow indicates a GABAnegative neuron positive for NCAM and neurocan, and the green neuron represents a GABAergic interneuron. Scale bar=10 μm.

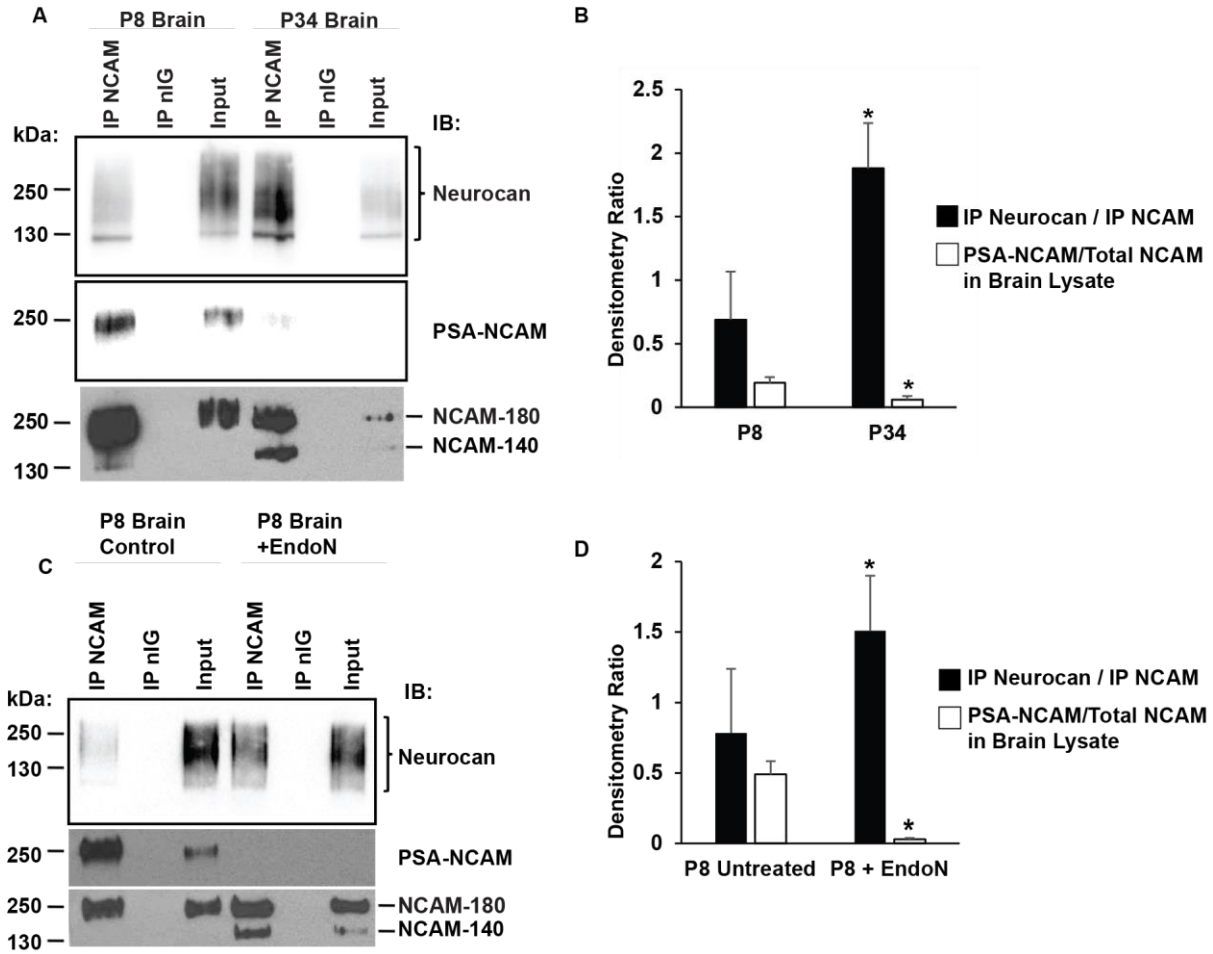

Figure 13: PSA inhibits binding of NCAM to neurocan. (A) Co-immunoprecipitation of neurocan and NCAM from P8 or P34 brain extracts immunoblotted for neurocan, NCAM, and PSA-NCAM. (B) Densitometry of (A). Graph indicates the ratio of bound neurocan to immunoprecipitated NCAM using black bars and ratio of PSA-NCAM to total NCAM in brain lysate (white bars) (n=3, t-test, * $p<0.05$). (C) Coimmunoprecipitation of neurocan and NCAM from untreated or EndoN-treated brain extracts immunoblotted for neurocan, NCAM, and PSA-NCAM. (D) Densitometry of (C). Graph indicates the ratio of bound neurocan to immunoprecipitated NCAM (black bars) and ratio of PSA-NCAM to total NCAM in brain lysate (white bars) (n=3, t-test, * $p<0.05$).

Neurocan binds to the Ig2 domain of NCAM

NCAM contains a heparin sulfate proteoglycan (HSPG) binding site in its Ig2 domain,[12] and residues within this proteoglycan binding domain (R156 and K162) are required for EphA3 binding.[27] Because the CSPG neurocan and HSPGs are extensively modified by GAG chain addition, it was hypothesized that neurocan engages the NCAM extracellular region (NCAM-EC) within the Ig2 proteoglycan binding domain. The neurocan binding site on NCAM was identified using assays in which Fc fusion proteins consisting of human NCAM Ig1-5/FN1-2

(full-length NCAM-EC), Ig1-3, Ig1-2, Ig2, and Ig1 (or Fc alone as a control) were incubated with recombinant human neurocan, and then pulled down with Protein A/G-Sepharose beads. Results showed that neurocan bound most effectively to full-length NCAM-EC and NCAM Ig2 (Fig. 14A,B). Neurocan bound to a lesser extent to NCAM truncation fragments Ig1-3, Ig 1-2, and Ig1 (50%, 33%, and 23% compared to NCAM-EC-Fc binding, respectively) (Fig. 14A,B). Quantification of binding showed that neurocan binding to NCAM Ig2-Fc was greater than to NCAM-EC (129% compared to amount of neurocan bound to NCAM-EC-Fc) (Fig. 14A,B). Apart from Ig1-Fc, all other constructs tested contained the Ig2 domain but bound with varying affinities to neurocan. Structural studies suggest that NCAM forms dimers through *cis* interactions between its Ig1 and Ig2 domains[28] and also *trans* interactions involving Ig3. The presence or absence of various Ig domains may influence the ability of NCAM to dimerize in solution, affecting accessibility of the Ig2 binding site of neurocan and potentially resulting in different affinities for neurocan binding. As the NCAM Ig2-Fc fragment is free from dimer-induced steric hindrance by Ig1 or Ig3, it may be more accessible for neurocan binding, which is consistent with the binding results.

Neurocan contains a carboxyl terminal sushi domain, a structure known to mediate protein-protein interactions. NCAM binds EphA3 at its cysteine-rich-domain (CRD), which also contains a sushi domain.[27] The Ig family member, L1-CAM, interacts with the sushi domain of neurocan.[29] Thus, it was hypothesized that the sushi domain of neurocan might be involved in NCAM/neurocan binding. The contribution of the neurocan sushi domain to NCAM binding was tested using recombinant human neurocan (full-length protein) or mouse neurocan Glu23-637 (a truncation lacking the sushi domain). These recombinant neurocan proteins were incubated with human NCAM-EC-Fc, and the amount of bound neurocan was assessed after Fc-pulldown. Both

mouse and human neurocan bound efficiently to NCAM-EC-Fc. Binding of mouse neurocan lacking the sushi domain was somewhat decreased compared to full-length neurocan (93% relative to human neurocan level bound to NCAM), but this difference was not statistically significant ($p = 0.23$, t-test) (Fig. 14C).

A complementary charged interface between the extracellular NCAM Ig2 domain and the EphA3 CRD mediates the binding and clustering of NCAM and EphA3 in the neuronal membrane. Amino acids R156 and K162 in the NCAM Ig2 domain were identified by molecular modeling and determined to be important residues for NCAM binding to EphA3.[27] These residues are also part of a domain required for NCAM binding to heparin sulfate proteoglycans (HSPGs).[28] In contrast, another Ig2 residue (NCAM R192) is not within the EphA3 binding site.[27] To assess the contribution of residues in NCAM Ig2 to neurocan binding, lysates of HEK293T cells expressing wild type (WT) NCAM or NCAM mutants (R156E, K162D, and R192E) were incubated with full-length neurocan, and the amount of neurocan co-immunoprecipitating with NCAM was analyzed by immunoblotting. Neurocan co-immunoprecipitated with WT NCAM and NCAM R192E, but bound to a much lesser extent with NCAM R156E and K162D mutants (32% and 41% of WT) (Fig. 14D,E, $p < 0.05$). These results indicate that neurocan binding to NCAM Ig2 involves residues involved in EphA3 association and HSPG binding.

Neurocan GAG chains mediate NCAM binding and disrupt the NCAM/EphA3 interaction

The shared NCAM binding site of neurocan and EphA3 led us to the hypothesis that competitive binding may occur between these proteins. To assess the ability of neurocan to disrupt NCAM/EphA3 binding and to test the importance of GAG chains in this process, a cell-culture binding assay was developed. Conditions were established to pre-treat recombinant

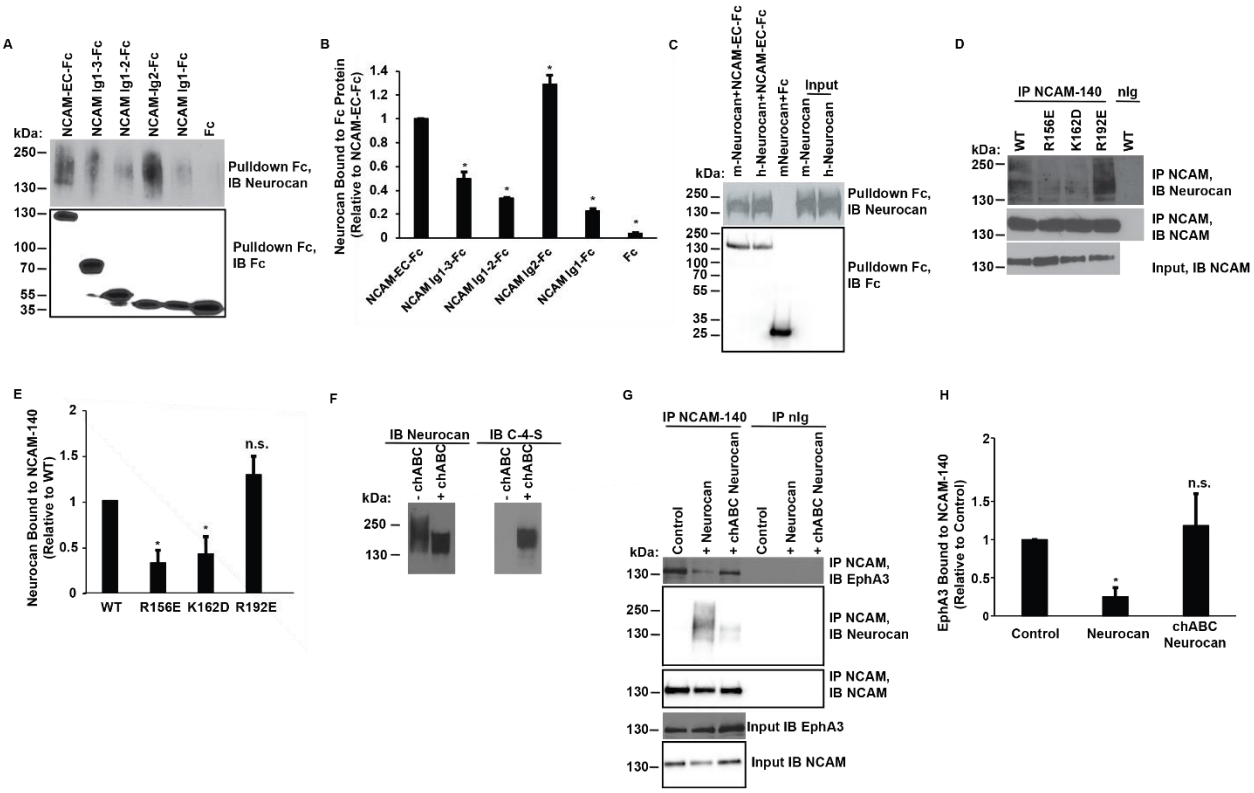

Figure 14: Neurocan binds the Ig2 domain of NCAM, decreasing EphA3 binding. (A) Fc pulldowns of the NCAM extracellular domain (NCAM-EC), truncation mutants of NCAM, or control Fc and recombinant neurocan. (B) Densitometry of (A) indicating the level of neurocan bound (relative to positive control NCAM-EC-Fc bound neurocan) for each construct (* $p<0.05$ compared to NCAM-EC-Fc) (C) Fc-pulldowns of NCAM-EC-Fc or control Fc with mouse neurocan (lacking sushi domain) and full-length human neurocan. (D) Co-immunoprecipitation of WT NCAM-140 or mutants of NCAM and neurocan from transfected HEK293T cells. (E) Densitometry of (D). The amount of coimmunoprecipitated neurocan for each NCAM IP was normalized to control WT NCAM bound neurocan (n=3, t-test, * $p<0.05$). (F) Immunoblot of untreated or chABC-treated neurocan protein probed for neurocan or C-4-S. (G) Co-immunoprecipitation of NCAM-140 and EphA3 from transfected HEK293 cells treated with no neurocan (control), neurocan, or chABC-treated neurocan. (H) Densitometry of (G). The amount of co32 immunoprecipitated EphA3 for each NCAM IP was normalized to control NCAM-bound EphA3 (n=3, t-test, * $p<0.05$).

neurocan with chABC followed by heat inactivation of enzyme. The efficiency of GAG removal was confirmed by a loss of high molecular weight GAG-modified neurocan by SDS-PAGE (Fig. 14F).

Further confirmation of chABC efficacy was obtained by immunoblotting for chondroitin-4-sulfate (C-4-S) stubs which are generated after chABC treatment. C-4-S signal was observed after chABC treatment but not in control sample processed without enzyme, indicating that chABC treatment was effective (Fig. 14F). HEK293T cells expressing non-PSA

NCAM-140 and EphA3 were treated with neurocan, chABC-pretreated neurocan, or left untreated prior to lysis. NCAM-140 was immunoprecipitated, and the amounts of bound EphA3 and neurocan were analyzed by immunoblotting. EphA3 binding was significantly decreased to a level of 25% of control in neurocan-treated cells ($p < 0.05$), but chABC-treated neurocan did not significantly alter EphA3 binding ($p > 0.05$) (Fig. 14G,H). Furthermore, after chABC treatment, 69% less neurocan was bound to non-PSA NCAM-140 compared to control neurocan (Fig. 14G, $p < 0.05$). These results indicated that neurocan decreased binding of EphA3 to non-PSA NCAM, and that neurocan/NCAM binding required intact GAG chains of neurocan.

Neurocan inhibits Ephrin-A5-induced clustering/activation of NCAM and EphA3 in cultured cortical interneurons

The activation of Eph receptor signaling is initiated by ephrin-induced receptor oligomerization in the plasma membrane.[30] Mechanistically, NCAM promotes ephrin-A-induced repulsion in GABAergic neurons by stimulating EphA3 receptor clustering, tyrosine kinase activation, and signaling through the small GTPase RhoA.[27] NCAM has been shown to co-cluster with EphA3 and to potentiate oligomerization in processes of GABAergic interneurons in cortical cultures.[27] The effect of neurocan on ephrin-A5-induced clustering of endogenous NCAM and EphA3 was assessed in mouse cortical cultures using this assay.[27] Neuronal cultures (14 DIV) were incubated with or without recombinant neurocan (4 nM, 30 minutes) before stimulation with control Fc or ephrin-A5-Fc for 30 minutes. Immunostaining of NCAM, EphA3, and GABA (to identify interneurons) was performed after cell fixation. Co-clustering of NCAM and EphA3 was analyzed in confocal images in which only GABA-labeled regions of interest (ROIs) were selected using ImageJ co-localization software. Results of the analysis yielded Pearson's Correlation Coefficients (R-Total), ranging from −1 (no correlation) to 1 (absolute correlation). In untreated cells, ephrin-A5-Fc induced strong co-localization of NCAM and

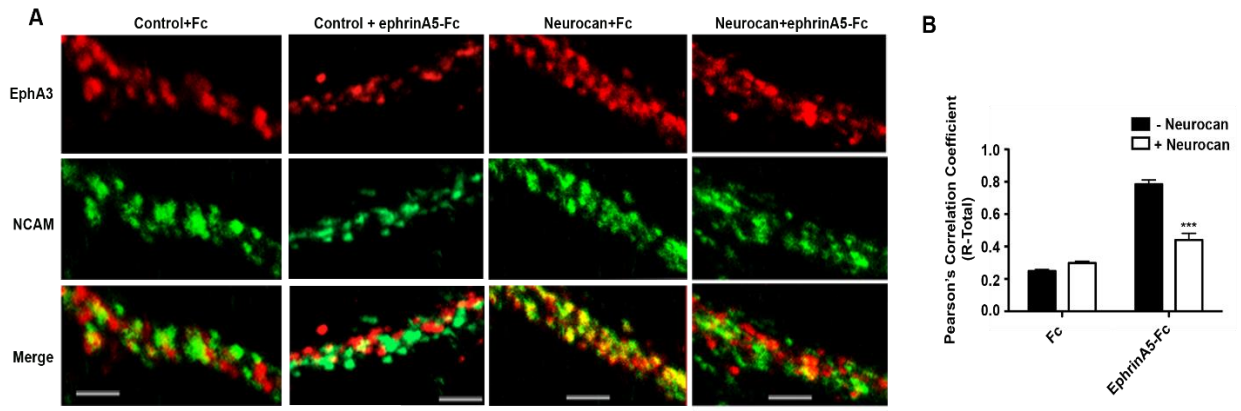

Figure 15: Neurocan impairs ephrin-A5-mediated clustering of NCAM and EphA3 in cortical interneurons in culture. (A) Cortical neuron cultures were pretreated with no neurocan (control) or neurocan followed by preclustered Fc or ephrin-A5-Fc, and localization of endogenous NCAM (green) and EphA3 (red) was assessed in axons of GABA immunopositive axons by confocal microscopy. Scale bars = 5 μM. (B) Pearson's Correlation Coefficients (R-Total) were generated for each condition using ImageJ colocalization software (n=3, two-way ANOVA with Bonferonni post-hoc testing, * $p<0.05$).

EphA3 as seen in merged images and a 4-fold increase in R-Total (Fig. 15A,B). In contrast, ephrin-A5-induced co-localization of NCAM and EphA3 in neurocan-treated cells was significantly reduced (Fig. 15A,B). These findings show that neurocan can block NCAM/EphA3 co-clustering on GABAergic neuronal processes, in accord with its ability to perturb binding.

Ephrin-A-induced clustering of EphA receptors induces autophosphorylation of tyrosine residues in the receptor cytoplasmic domain[31,32] leading to downstream signaling. To evaluate the consequences of neurocan on EphA3 kinase activation, EphA3 autophosphorylation was assessed in HEK293T cells co-expressing NCAM-140 and EphA3. Cells were treated with or without neurocan (20 nM, 30 minutes), then stimulated with control Fc or ephrin-A5-Fc. EphA3 was immunoprecipitated and immunoblotted with phosphotyrosine antibody (PY99), followed by stripping and reprobing for EphA3 protein. The ratio of phospho-EphA3 to total EphA3 was quantified by densitometry and compared for significant differences. In control cultures treated with ephrin-A5-Fc, EphA3 phosphorylation was strongly increased in comparison to Fc treated cells (Fig. 16A,B). In neurocan-treated cells, ephrin-A5-induced EphA3 autophosphorylation was effectively blocked (Fig. 16A,B). Binding of neurocan to other components of the

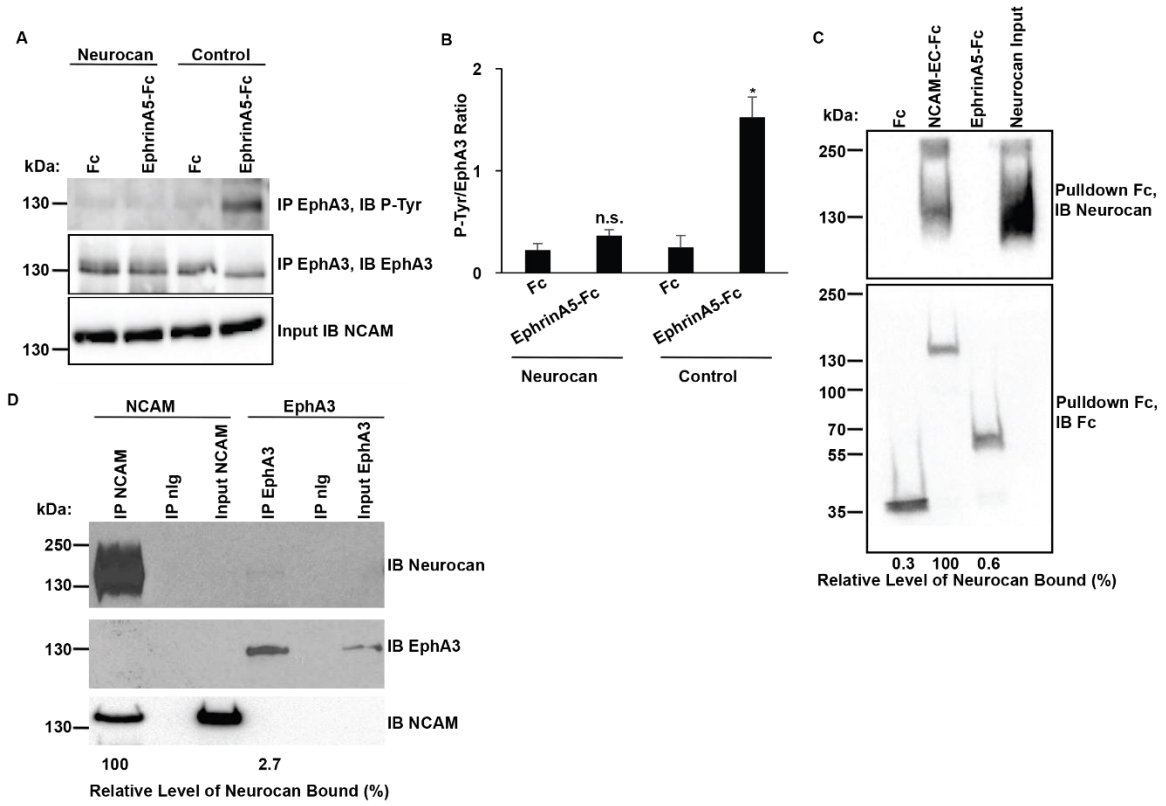

Figure 16: Neurocan decreases ephrin-A5-induced EphA3 autophosphorylation. (A) HEK293T cells transfected with NCAM and EphA3 were treated with preclustered control Fc or ephrin-A5-Fc, and EphA3 was immunoprecipitated. EphA3 autophosphorylation was assessed by immunoblotting with a phosphotyrosine antibody (PY99). Total levels of immunoprecipitated EphA3 were assessed by reprobing with EphA3 antibody. (B) Densitometry of (A). Graph indicates the ratio of phosphotyrosine to EphA3 values for each condition (n=3, * $p<0.05$). (C) Fc-pulldowns of control Fc, NCAM-EC-Fc, and ephrin-A5-Fc with recombinant neurocan. Level of neurocan bound (relative to positive control NCAM-EC-Fc bound neurocan) is indicated as a percentage under each lane. (D) Co-immunoprecipitation of NCAM (positive control) or EphA3 with neurocan from transfected HEK293T cells. Level of neurocan bound (relative to positive control NCAM-EC-Fc bound neurocan) is indicated as a percentage under each lane.

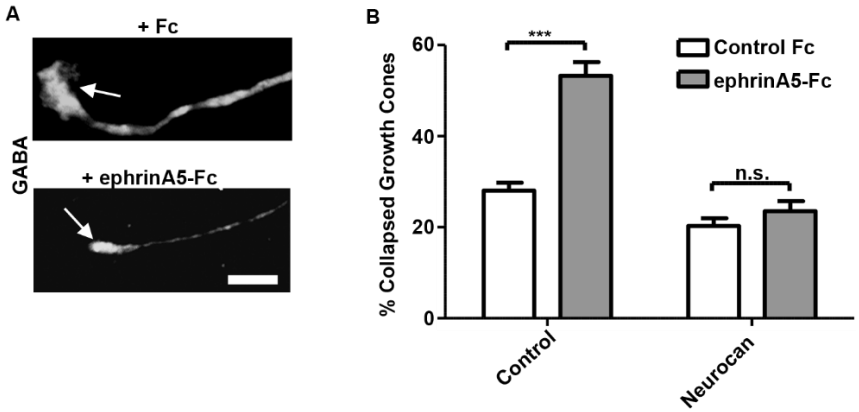

Figure 17: Neurocan inhibits ephrin-A5-induced growth cone collapse in GABAergic interneurons. (A) Representative spread and collapsed growth cones of GABA33 immunostained interneurons in cortical neuron cultures. Scale bar = 5 μM. (B) The percentage of collapsed growth cones was determined for each condition (300 growth cones per condition, n=3 experiments, 2-way ANOVA, Bonferonni post-hoc testing, *** $p<0.001$).

NCAM/EphA3/ephrin-A5 signaling complex was also assessed. In pull down assays, purified recombinant neurocan bound to NCAM-EC-Fc but did not bind ephrin-A5-Fc (relative level of neurocan bound to EphrinA5-Fc was 0.6% of neurocan bound to NCAM-EC-Fc, $n = 3$, $p < 0.05$) (Fig. 16C). Results of co-immunoprecipitation from HEK293T cells expressing NCAM140 or EphA3 indicated that neurocan bound to NCAM but not to EphA3 (relative level of neurocan bound to EphA3 was 2.7% of neurocan bound to NCAM, $n = 3$, $p < 0.05$) (Fig. 16D). Together, these results indicated that neurocan engages NCAM at the same extracellular motif required for EphA3 binding, inhibiting ephrin-A5-induced receptor clustering and EphA3 receptor activation.

Neurocan perturbs Ephrin-A5-induced growth cone collapse of GABAergic interneurons

Growth cone collapse in cultured neuronal cells is widely used for characterization of ephrin/Eph repellent responses.[33-35] Growth cone collapse of wild type (WT) versus NCAM null GABAergic neurons in culture closely correlates with perisomatic synapse densities in WT and NCAM null mice.[5,27] NCAM is required for ephrin-A5-mediated growth cone collapse of GABAergic interneurons in vitro,[5,27] but neurocan has not been tested for inhibition of this repellent response. To assess the effect of neurocan on ephrin-A5-induced growth cone collapse, mouse cortical neuron cultures (14 DIV) were treated with or without neurocan (4 nM, 30 min). Neurons were then stimulated with pre-clustered Fc or ephrin-A5-Fc for 30 minutes, and cultures were fixed and immunostained for GABA to identify interneurons. Neuronal growth cones of GABA-positive interneurons were scored as collapsed (bullet-shaped) or not collapsed (fan-shaped) based on morphology as described.[5,27] Ephrin-A5-Fc induced robust growth cone collapse (~55%) in untreated GABA-positive neurons, and this response was fully blocked in cells treated with neurocan (Fig. 17A,B). A fraction of neuronal cells were refractive to ephrin-A5-induced collapse, and may represent a subpopulation that does not express ephrin-A5

receptors, NCAM, and/or required signaling effectors. These results demonstrate that neurocan is capable of blocking ephrin-A5-induced repellent signaling in cortical interneurons. In combination with the effect of chABC on interneuron perisomatic synapse density in slice cultures, this functional assay supports a role for neurocan in inhibitory synapse maturation in vivo through inhibition of axonal repellent responses.

DISCUSSION

Here we identify a previously unknown role for the PNN protein neurocan in disrupting NCAM interaction with EphA3 to terminate repellent responses and limit the number of perisomatic inhibitory synapses made by basket interneurons onto pyramidal neurons in the mouse PFC. Targeting GAG chains of PNN proteins using the enzyme chABC decreased perisomatic synapse numbers in PFC layers 2,3 of organotypic brain slices, highlighting a previously unknown role for PNNs in regulating inhibitory synapse density of PV^+ interneurons in the PFC. Furthermore, neurocan was able to rescue the observed effects of chABC treatment. The present study further shows that neurocan perturbs NCAM/EphA3 receptor clustering by binding to the same critical determinants in the NCAM Ig2 domain that are required for binding to EphA3. As a consequence, neurocan inhibits EphA3 kinase activation and impairs ephrin-A5-induced growth cone collapse in GABAergic neurons. During postnatal stages of developmental synapse remodeling in the PFC, neurocan accumulated in the extracellular space and was closely associated with excitatory and inhibitory neurons. Neurocan was observed in close apposition with inhibitory perisomatic terminals by light and electron microscopy, but it did not colocalize within synapses.

Removal of the GAG chains of PNN proteins resulted in a decrease in GABAergic perisomatic synapse density in cortical organotypic slice cultures. The current binding studies and previous work suggest that this effect is unlikely to derive from an effect on NCAM binding to other PNN proteins, although experiments knocking down individual PNN components could be informative. A recent study showed that brevican promotes maturation of excitatory synapses contacting the soma of PV^+ interneurons,[36] thus different PNN components may regulate perisomatic synapses in distinct neuronal cell types.

Polysialylation of NCAM is associated with synaptic plasticity and remodeling of perisomatic synapses.[5,37] Neurocan interacted robustly with non-PSA NCAM isoforms but not with PSA-NCAM. The finding that PSA inhibited NCAM binding to neurocan suggests that polysialylation is a critical modification that allows remodeling during early development, which is later halted by the loss of PSA that occurs during maturation to terminate developmental plasticity. Developmental regulation of NCAM polysialylation may mediate the transition between remodeling of excess basket cell axon terminals and their stabilization at perisomatic synapses by modulating interaction with neurocan. Domain truncation analysis of NCAM mapped the key interaction site to the NCAM Ig2 domain. While the sushi domain of neurocan is essential for binding to L1,[29] this domain was not required for binding to NCAM. An interface involving complementary charged residues in the interacting domains of NCAM (Ig2) and EphA3 (CRD)[27] was found to mediate NCAM binding to neurocan. Basic residues in NCAM Ig2 (R156 and K162) were essential for interaction of NCAM with both neurocan and EphA3. These residues are positioned within the heparin-binding site of NCAM, which is essential for interaction of NCAM with extracellular matrix HSPGs.[38] Neurocan binding to NCAM at the heparin binding site (which also has affinity for CSPGs)[39] may promote cell-matrix adhesion as a necessary step for synapse stabilization at pyramidal cell soma. This interpretation is compatible with the decreased numbers of perisomatic synapses observed after chABC treatment.

Pulldown experiments with purified proteins demonstrated direct binding of NCAM to neurocan, but not to ephrin-A5 or EphA3. Neurocan interaction with NCAM was strongly dependent on GAG chains, but even the core protein of neurocan retained some binding affinity for NCAM. Neurocan blocked co-clustering of NCAM and EphA3 receptors on processes of cortical interneurons stimulated with the ligand ephrin-A5, suggesting that neurocan binding to

NCAM in the plasma membrane displaces EphA3. Neurocan treatment also inhibited ephrin-dependent EphA3 autophosphorylation. As clustering of EphA receptors is essential for kinase activation and downstream signaling at localized sites in the neuronal membrane,[30] the finding that neurocan can destabilize EphA3 clusters reveals an additional level of regulation in modulating ephrin-dependent repellent activity.

In a functional assay of ephrin-dependent signaling, neurocan significantly perturbed ephrin-A5-dependent growth cone collapse. Because NCAM is required for ephrin-A5-dependent growth cone collapse of cortical interneurons,[3,27] results are consistent with the interpretation that neurocan/NCAM interactions impair EphA3 clustering and downstream signaling to inhibit ephrin-A-induced axonal repellent responses. Although growth cone collapse *in vitro* correlates with inhibitory synapse densities observed *in vivo*,[5] the culture assay does not distinguish ephrin-A5-induced growth cone repulsion from elimination of nascent synaptic contacts. To address this question, live imaging of perisomatic synapse formation and elimination *in vivo* could be informative.

This study delineates a novel molecular mechanism in which neurocan disrupts NCAM/EphA3 receptor clustering, EphA3 tyrosine kinase activation, and repellent responses of axon terminals in interneurons in the developing PFC. Results support a model (Fig. 18) in which PSA-NCAM enables NCAM/EphA3 clustering and signaling to eliminate excess presynaptic contacts of PV^+ interneurons with pyramidal cell soma in early postnatal development. Upon maturation, neurocan in the forming PNNs binds to accumulating non-PSA NCAM, inhibiting ephrinA5/EphA3-mediated repellent responses and stabilizing inhibitory perisomatic synapses (Fig. 8). NCAM and EphA3 are both prominently involved in development of the nervous system, and neurocan is a potential risk factor in schizophrenia[40] and bipolar

disorder[41]. Therefore, understanding how the PNN component neurocan influences the function of NCAM and EphA3 is relevant to both normal development and disease states.

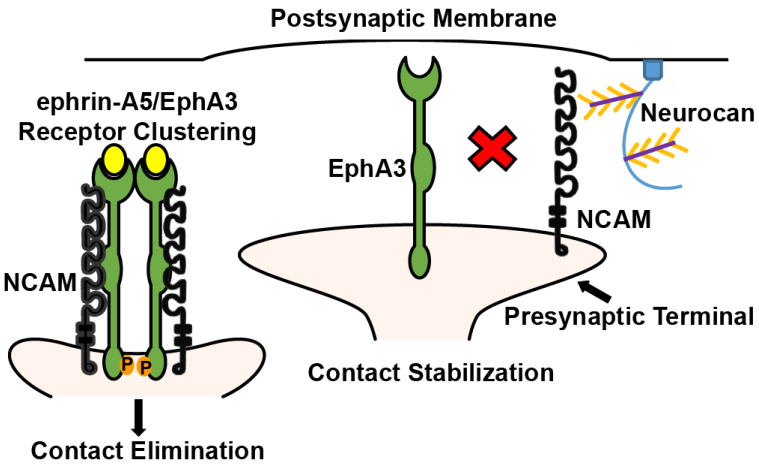

Figure 18: Model of inhibition of NCAM/EphA3 clustering and activation by neurocan. During postnatal remodeling of transient perisomatic synapses made by PV+ interneurons onto pyramidal cell soma, ephrin-A5 dimers bind the ligand binding domains (LBD) of an EphA3 dimer. NCAM clusters the EphA3 receptors through binding of the NCAM Ig2 domain to the EphA3 CRD. EphA3 clustering activates tyrosine kinase signaling leading to synapse retraction. With further maturation, neurocan in PNNs engages the Ig2 domain of non-PSA NCAM, inhibiting EphA3 clustering and retraction of inhibitory perisomatic contacts. NCAM is shown in black, EphA3 is green, and ephrin-A5 is yellow. Neurocan core protein is depicted in purple with GAG chains in orange on a PNN scaffold (blue). P = phosphorylation. The illustration was created by modifying images purchased in the PPT Drawing Toolkits-BIOLOGY Bundle from Motifolio, Inc.

REFERENCES

Hippenmeyer, S. *et al.* (2005) A developmental switch in the response of DRG neurons to ETS transcription factor signaling. *PLoS Biol* **3**, e159.

Madisen, L. *et al*. (2010) A robust and high-throughput Cre reporting and characterization system for the whole mouse brain. *Nat Neurosci* **13**, 133-140.

Meiri, K. F., Saffell, J. L., Walsh, F. S. & Doherty, P. (1998) Neurite outgrowth stimulated by neural cell adhesion molecules requires growth-associated protein-43 (GAP-43) function and is associated with GAP-43 phosphorylation in growth cones. *J Neurosci* **18**, 10429-10437.

El Maarouf, A. & Rutishauser, U. (2003) Removal of polysialic acid induces aberrant pathways, synaptic vesicle distribution, and terminal arborization of retinotectal axons. *J Comp Neurol* **460**, 203-211.

Brennaman, L. H. *et al.* (2013). Polysialylated NCAM and ephrinA/EphA regulate synaptic development of GABAergic interneurons in prefrontal cortex. *Cereb Cortex* **23**, 162-177.

Chattopadhyaya, B. *et al.* (2011) Experience and activity-dependent maturation of perisomatic GABAergic innervation in primary visual cortex during a postnatal critical period. *J Neurosci* **24**, 9598-9611.

Balmer, T. S. (2016) Perineuronal Nets Enhance the Excitability of Fast-Spiking Neurons. *eNeuro* **3**.

Kim, K. K., Adelstein, R. S. & Kawamoto, S. (2009) Identification of neuronal nuclei (NeuN) as Fox-3, a new member of the Fox-1 gene family of splicing factors. *J Biol Chem* **284**, 31052-31061.

Yue, X., Son, A. I. & Zhou, R. (2013) Growth cone collapse assay**. *Methods Mol Biol* 1018**, 221-227.

Hinkle, C. L., Diestel, S., Lieberman, J. & Maness, P. F. (2006) Metalloprotease-induced ectodomain shedding of neural cell adhesion molecule (NCAM). *Journal of Neurobiology* **66**, 1378-1395.

Brennaman, L. H. & Maness, P. F. (2008) Developmental regulation of GABAergic interneuron branching and synaptic development in the prefrontal cortex by soluble neural cell adhesion molecule. *Mol Cell Neurosci* **37**, 781-793.

Sullivan, C. S., Kumper, M., Temple, B. S. & Maness, P. F. (2016) The Neural Cell Adhesion Molecule (NCAM) Promotes Clustering and Activation of EphA3 Receptors in GABAergic Interneurons to Induce Ras Homolog Gene Family, Member A (RhoA)/Rho-

associated protein kinase (ROCK)-mediated Growth Cone Collapse. *J Biol Chem* **291**, 26262-26272.

Yizhar, O. *et al.* (2011) Neocortical excitation/inhibition balance in information processing and social dysfunction. *Nature* **477**, 171-178.

Hamilton, D. A. & Brigman, J. L. (2015) Behavioral flexibility in rats and mice: contributions of distinct frontocortical regions. *Genes Brain Behav* **14**, 4-21.

Hartig, W., Brauer, K. & Bruckner, G. (1992) Wisteria floribunda agglutinin-labelled nets surround parvalbumin-containing neurons. *Neuroreport* **3**, 869-872.

Yang, S. *et al.* (2015) Perineuronal net digestion with chondroitinase restores memory in mice with tau pathology. *Exp Neurol* **265**, 48-58.

Friedlander, D. R. *et al.* (1994) The neuronal chondroitin sulfate proteoglycan Neurocan binds to the neural cell adhesion molecules Ng-CAM/L1/NILE and N-CAM, and inhibits neuronal adhesion and neurite outgrowth. *J Cell Biol* **125**, 669-680.

Milev, P. *et al.* (1994) Interactions of the chondroitin sulfate proteoglycan phosphacan, the extracellular domain of a receptor-type protein tyrosine phosphatase, with neurons, glia, and neural cell adhesion molecules. *J Cell Biol* **127**, 1703-1715.

Deepa, S. S. *et al.* (2006) Composition of perineuronal net extracellular matrix in rat brain: a different disaccharide composition for the net-associated proteoglycans. *J Biol Chem* **281**, 17789-17800.

Nikonenko, A., Schmidt, S., Skibo, G., Bruckner, G. & Schachner, M. (2003) Tenascin-R-deficient mice show structural alterations of symmetric perisomatic synapses in the CA1 region of the hippocampus. *J Comp Neurol* **456**, 338-349.

Saghatelyan, A. K. *et al.* (2000) The extracellular matrix molecule tenascin-R and its HNK-1 carbohydrate modulate perisomatic inhibition and long-term potentiation in the CA1 region of the hippocampus. *Eur J Neurosci* **12**, 3331-3342.

Saghatelyan, A. K. *et al.* (2001) Reduced perisomatic inhibition, increased excitatory transmission, and impaired long-term potentiation in mice deficient for the extracellular matrix glycoprotein tenascin-R. *Mol Cell Neurosci* **17**, 226-240.

Saghatelyan, A. K. *et al.* (2003) Recognition molecule associated carbohydrate inhibits postsynaptic GABA(B) receptors: a mechanism for homeostatic regulation of GABA release in perisomatic synapses. *Mol Cell Neurosci* **24**, 271-282.

Sytnyk, V., Leshchyns'ka, I. & Schachner, M. (2017) Neural Cell Adhesion Molecules of the Immunoglobulin Superfamily Regulate Synapse Formation, Maintenance, and Function. *Trends Neurosci* **40**, 295-308.

Goebbels, S. *et al.* (2006)Genetic targeting of principal neurons in neocortex and hippocampus of NEX-Cre mice. *Genesis* **44**, 611-621.

Kallapur, S. G. & Akeson, R. A. (1992) The neural cell adhesion molecule (NCAM) heparin binding domain binds to cell surface heparan sulfate proteoglycans. *Journal of neuroscience research* **33**, 538-548.

Soroka, V., Kasper, C. & Poulsen, F. M. (2010) Structural biology of NCAM. *Adv Exp Med Biol* **663**, 3-22.

Oleszewski, M., Gutwein, P., von der Lieth, W., Rauch, U. & Altevogt, P. (2000) Characterization of the L1-neurocan-binding site. Implications for L1-L1 homophilic binding. *J Biol Chem* **275**, 34478-34485.

Kania, A. & Klein, R. (2016)Mechanisms of ephrin-Eph signalling in development, physiology and disease. *Nat Rev Mol Cell Biol* **17**, 240-256.

Shi, G., Yue, G. & Zhou, R. (2010) EphA3 functions are regulated by collaborating phosphotyrosine residues. *Cell Res* **20**, 1263-1275.

Davis, T. L. *et al.* (2008) Autoregulation by the juxtamembrane region of the human ephrin receptor tyrosine kinase A3 (EphA3). *Structure* **16**, 873-884.

Wong, E. V., Kerner, J. A. & Jay, D. G. (2004) Convergent and divergent signaling mechanisms of growth cone collapse by ephrinA5 and slit2. *J Neurobiol* **59**, 66-81.

Dudanova, I., Gatto, G. & Klein, R. (2010) GDNF acts as a chemoattractant to support ephrinA-induced repulsion of limb motor axons. *Curr Biol* **20**, 2150-2156.

Demyanenko, G. P. *et al.* (2011) L1 and CHL1 Cooperate in Thalamocortical Axon Targeting. *Cereb Cortex* **21**, 401-412.

Favuzzi, E. *et al*. (2017) Activity-Dependent Gating of Parvalbumin Interneuron Function by the Perineuronal Net Protein Brevican. *Neuron* **95**, 639-655.

Di Cristo, G. *et al.* (2007) Activity-dependent PSA expression regulates inhibitory maturation and onset of critical period plasticity. *Nat Neurosci* **10**, 1569-1577.

Cole, G. J. & Akeson, R. (1989) Identification of a heparin binding domain of the neural cell adhesion molecule N-CAM using synthetic peptides. *Neuron* **2**, 1157-1165.

Kulahin, N. *et al.* (2005) Modulation of the homophilic interaction between the first and second Ig modules of neural cell adhesion molecule by heparin. *J Neurochem* **95**, 46-55.

Brennaman, L. H., Moss, M. L. & Maness, P. F. (2014) EphrinA/EphA-induced ectodomain

shedding of neural cell adhesion molecule regulates growth cone repulsion through ADAM10 metalloprotease. *J Neurochem* **128**, 267-279.

Schultz, C. C. *et al*. (2014) Common variation in NCAN, a risk factor for bipolar disorder and schizophrenia, influences local cortical folding in schizophrenia. *Psychol Med* **44**, 811-820.

Cichon, S. *et al*. (2011) Genome-wide association study identifies genetic variation in neurocan as a susceptibility factor for bipolar disorder. *Am J Hum Genet* **88**, 372-381.